Whether FDC markers are positive or not, a longer follow-up is necessary for patients with EBV-positive IPTs than for those with EBV-negative IPTs. Cheuk et al [7] reported three cases of recurrence in the liver, hemidiaphragm and ascending colon, one case of regional lymph node metastasis, and one case of peritoneal dissemination among patients with IPT-like FDC tumours in the liver. Data regarding the recurrence or metastasis of splenic lesions following splenectomy are not yet available; however, a longer follow-up period could provide detailed pathology of EBV-positive tumours in the spleen. IPT is widely recognized as a benign lesion; therefore, the concept of splenic EBV-positive tumours is required to attract clinicians' attention to these potentially malignant lesions.

Conclusions

In summary, we presented cases of EBV-positive IPT and an IPT-like FDC tumour in the spleen. We believe that they are of the same entity whether positive or negative for "conventional" FDC markers. No differences in clinicopathological features of imaging have been reported to date. For the time being, they should be clinically evaluated, treated and followed up in the same manner.

References

1. Dalal BI, Greenberg H, Quinonez GE, Gough JC. Inflammatory pseudotumor of the spleen. Morphological, radiological, immunophenotypic, and ultrastructural features. Arch Pathol Lab Med 1991;115:1062–4.
2. Yamaguchi M, Yamamoto T, Tate G, Matsumoto T, Matsumiya A, Kuzume M, et al. Specific detection of epstein-barr virus in inflammatory pseudotumor of the spleen in a patient with a high serum level of soluble IL-2 receptor. J Gastroenterol 2000;35:563–6.
3. Arber DA, Kamel OW, van de Rijn M, Davis RE, Medeiros LJ, Jaffe ES, et al. Frequent presence of the Epstein-Barr virus in inflammatory pseudotumor. Hum Pathol 1995;26:1093–8.
4. Oz Puyan F, Bilgi S, Unlu E, Yalcin O, Altaner S, Demir M, et al. Inflammatory pseudotumor of the spleen with EBV positivity: report of a case. Eur J Haematol 2004;72:285–91.
5. Akatsu T, Kameyama K, Tanabe M, Endo T, Kitajima M. Epstein-Barr virus-positive inflammatory pseudotumor of the spleen with concomitant rectal cancer: a case report and review of the literature. Dig Dis Sci 2007;52:2806–12.
6. Araujo VC, Martins MT, Salmen FS, Araujo NS. Extranodal follicular dendritic cell sarcoma of the palate. Oral Surg Oral Med Oral Pathol Oral Radiol Endod 1999;87:209–14.
7. Cheuk W, Chan JK, Shek TW, Chang JH, Tsou MH, Yuen NW, et al. Inflammatory pseudotumor-like follicular dendritic cell tumor: a distinctive low-grade malignant intra-abdominal neoplasm with consistent Epstein-Barr virus association. Am J Surg Pathol 2001;25:721–31.
8. Perez-Ordonez B, Erlandson RA, Rosai J. Follicular dendritic cell tumor: report of 13 additional cases of a distinctive entity. Am J Surg Pathol 1996;20:944–55.
9. Horiguchi H, Matsui-Horiguchi M, Sakata H, Ichinose M, Yamamoto T, Fujiwara M, et al. Inflammatory pseudotumor-like follicular dendritic cell tumor of the spleen. Pathol Int 2004;54:124–31.
10. Shek TW, Ho FC, Ng IO, Chan AC, Ma L, Srivastava G. Follicular dendritic cell tumor of the liver. Evidence for an Epstein-Barr virus-related clonal proliferation of follicular dendritic cells. Am J Surg Pathol 1996;20:313–24.
11. Brittig F, Ajtay E, Jakso P, Kelenyi G. Follicular dendritic reticulum cell tumor mimicking inflammatory pseudotumor of the spleen. Pathol Oncol Res 2004;10:57–60.
12. Monda L, Warnke R, Rosai J. A primary lymph node malignancy with features suggestive of dendritic reticulum cell differentiation. A report of 4 cases. Am J Pathol 1986;122:562–72.
13. Chan JK, Fletcher CD, Nayler SJ, Cooper K. Follicular dendritic cell sarcoma. Clinicopathologic analysis of 17 cases suggesting a malignant potential higher than currently recognized. Cancer 1997;79:294–313.
14. Perez-Ordonez B, Rosai J. Follicular dendritic cell tumor: review of the entity. Semin Diagn Pathol 1998;15:144–54.
15. Hollowood K, Stamp G, Zouvani I, Fletcher CD. Extranodal follicular dendritic cell sarcoma of the gastrointestinal tract. Morphologic, immunohistochemical and ultrastructural analysis of two cases. Am J Clin Pathol 1995;103:90–7.
16. Irie H, Honda H, Kaneko K, Kuroiwa T, Fukuya T, Yoshimitsu K, et al. Inflammatory pseudotumors of the spleen: CT and MRI findings. J Comput Assist Tomogr 1996;20:244–8.
17. Franquet T, Montes M, Aizcorbe M, Barberena J, Ruiz De Azua Y, Cobo F. Inflammatory pseudotumor of the spleen: ultrasound and computed tomographic findings. Gastrointest Radiol 1989;14:181–3.
18. Glazer M, Lally J, Kanzer M. Inflammatory pseudotumor of the spleen: MR findings. J Comput Assist Tomogr 1992;16:980–3.
19. Yamakado K, Matsuda A, Katoh N, Hirano T, Takeda K, Nakagawa T. Inflammatory pseudotumour of the spleen: CT and MRI findings. Eur Radiol 1994;4:271–3.
20. Ros PR, Moser RP Jr, Dachman AH, Murari PJ, Olmsted WW. Hemangioma of the spleen: radiologic-pathologic correlation in ten cases. Radiology 1987;162:73–7.
21. Wadsworth DT, Newman B, Abramson SJ, Carpenter BL, Lorenzo RL. Splenic lymphangiomatosis in children. Radiology 1997;202:173–6.
22. Ohtomo K, Fukuda H, Mori K, Minami M, Itai Y, Inoue Y. CT and MR appearances of splenic hamartoma. J Comput Assist Tomogr 1992;16:425–8.

nature Vol 459|4 June 2009|doi:10.1038/nature07969

LETTERS

Frequent inactivation of A20 in B-cell lymphomas

Motohiro Kato[1,2], Masashi Sanada[1,5], Itaru Kato[6], Yasuharu Sato[7], Junko Takita[1,2,3], Kengo Takeuchi[8], Akira Niwa[6], Yuyan Chen[1,2], Kumi Nakazaki[1,4,5], Junko Nomoto[9], Yoshitaka Asakura[9], Satsuki Muto[1], Azusa Tamura[1], Mitsuru Iio[1], Yoshiki Akatsuka[11], Yasuhide Hayashi[12], Hiraku Mori[13], Takashi Igarashi[2], Mineo Kurokawa[4], Shigeru Chiba[3], Shigeo Mori[14], Yuichi Ishikawa[8], Koji Okamoto[10], Kensei Tobinai[9], Hitoshi Nakagama[10], Tatsutoshi Nakahata[6], Tadashi Yoshino[7], Yukio Kobayashi[9] & Seishi Ogawa[1,5]

A20 is a negative regulator of the NF-κB pathway and was initially identified as being rapidly induced after tumour-necrosis factor-α stimulation[1]. It has a pivotal role in regulation of the immune response and prevents excessive activation of NF-κB in response to a variety of external stimuli[2–7]; recent genetic studies have disclosed putative associations of polymorphic *A20* (also called *TNFAIP3*) alleles with autoimmune disease risk[8,9]. However, the involvement of A20 in the development of human cancers is unknown. Here we show, using a genome-wide analysis of genetic lesions in 238 B-cell lymphomas, that *A20* is a common genetic target in B-lineage lymphomas. A20 is frequently inactivated by somatic mutations and/or deletions in mucosa-associated tissue lymphoma (18 out of 87; 21.8%) and Hodgkin's lymphoma of nodular sclerosis histology (5 out of 15; 33.3%), and, to a lesser extent, in other B-lineage lymphomas. When re-expressed in a lymphoma-derived cell line with no functional *A20* alleles, wild-type A20, but not mutant A20, resulted in suppression of cell growth and induction of apoptosis, accompanied by downregulation of NF-κB activation. The A20-deficient cells stably generated tumours in immunodeficient mice, whereas the tumorigenicity was effectively suppressed by re-expression of A20. In A20-deficient cells, suppression of both cell growth and NF-κB activity due to re-expression of A20 depended, at least partly, on cell-surface-receptor signalling, including the tumour-necrosis factor receptor. Considering the physiological function of A20 in the negative modulation of NF-κB activation induced by multiple upstream stimuli, our findings indicate that uncontrolled signalling of NF-κB caused by loss of A20 function is involved in the pathogenesis of subsets of B-lineage lymphomas.

Malignant lymphomas of B-cell lineages are mature lymphoid neoplasms that arise from various lymphoid tissues[10,11]. To obtain a comprehensive registry of genetic lesions in B-lineage lymphomas, we performed a single nucleotide polymorphism (SNP) array analysis of 238 primary B-cell lymphoma specimens of different histologies, including 64 samples of diffuse large B-cell lymphomas (DLBCLs), 52 follicular lymphomas, 35 mantle cell lymphomas (MCLs), and 87 mucosa-associated tissue (MALT) lymphomas (Supplementary Table 1). Three Hodgkin's-lymphoma-derived cell lines were also analysed. Interrogating more than 250,000 SNP sites, this platform permitted the identification of copy number changes at an average resolution of less than 12 kilobases (kb). The use of large numbers of SNP-specific probes is a unique feature of this platform, and combined with the CNAG/AsCNAR software, enabled accurate determination of 'allele-specific' copy numbers, and thus allowed for sensitive detection of loss of heterozygosity (LOH) even without apparent copy-number reduction, in the presence of up to 70–80% normal cell contamination[12,13].

Lymphoma genomes underwent a wide range of genetic changes, including numerical chromosomal abnormalities and segmental gains and losses of chromosomal material (Supplementary Fig. 1), as well as copy-number-neutral LOH, or uniparental disomy (Supplementary Fig. 2). Each histology type had a unique genomic signature, indicating a distinctive underlying molecular pathogenesis for different histology types (Fig. 1a and Supplementary Fig. 3). On the basis of the genomic signatures, the initial pathological diagnosis of MCL was re-evaluated and corrected to DLBCL in two cases. Although most copy number changes involved large chromosomal segments, a number of regions showed focal gains and deletions, accelerating identification of their candidate gene targets. After excluding known copy number variations, we identified 46 loci showing focal gains (19 loci) or deletions (27 loci) (Supplementary Tables 2 and 3 and Supplementary Fig. 4).

Genetic lesions on the NF-κB pathway were common in B-cell lymphomas and found in approximately 40% of the cases (Supplementary Table 1), underpinning the importance of aberrant NF-κB activation in lymphomagenesis[11,14] in a genome-wide fashion. They included focal gain/amplification at the *REL* locus (16.4%) (Fig. 1b) and *TRAF6* locus (5.9%), as well as focal deletions at the *PTEN* locus (5.5%) (Supplementary Figs 1 and 4). However, the most striking finding was the common deletion at 6q23.3 involving a 143-kb segment. It exclusively contained the *A20* gene (also called *TNFAIP3*), a negative regulator of NF-κB activation[3–7,15] (Fig. 1b), which was previously reported as a candidate target of 6q23 deletions in ocular lymphoma[16]. LOH involving the *A20* locus was found in 50 cases, of which 12 showed homozygous deletions as determined by the loss of both alleles in an allele-specific copy number analysis (Fig. 1b, Table 1 and Supplementary Table 4). On the basis of this finding, we searched for possible tumour-specific mutations of *A20* by genomic DNA sequencing of entire coding exons of the gene in the same series of lymphoma samples (Supplementary Fig. 5). Because two out of the three Hodgkin's-lymphoma-derived cell lines had biallelic *A20* deletions/mutations (Supplementary Fig. 6), 24 primary samples from Hodgkin's lymphoma were also analysed for mutations, where

[1]Cancer Genomics Project, Department of [2]Pediatrics, [3]Cell Therapy and Transplantation Medicine, and [4]Hematology and Oncology, Graduate School of Medicine, University of Tokyo, 7-3-1 Hongo, Bunkyo-ku, Tokyo 113-8655, Japan. [5]Core Research for Evolutional Science and Technology, Japan Science and Technology Agency, 4-1-8, Honcho, Kawaguchi-shi, Saitama 332-0012, Japan. [6]Department of Pediatrics, Graduate School of Medicine, Kyoto University, 54 Kawahara-cho, Shogoin, Sakyo-ku, Kyoto 606-8507, Japan. [7]Department of Pathology, Okayama University Graduate School of Medicine, Dentistry and Pharmaceutical Sciences, 2-5-1 Shikata-cho, Kita-ku, Okayama 700-8558, Japan. [8]Division of Pathology, The Cancer Institute of Japanese Foundation for Cancer Research, Japan, 3-10-6 Ariake, Koto-ku, Tokyo 135-8550, Japan. [9]Hematology Division, Hospital, and [10]Early Oncogenesis Research Project, Research Institute, National Cancer Center, 5-1-1 Tsukiji, Chuo-ku, Tokyo 104-0045, Japan. [11]Division of Immunology, Aichi Cancer Center Research Institute, 1-1 Kanokoden, Chikusa-ku, Nagoya 464-8681, Japan. [12]Gunma Children's Medical Center, 779 Shimohakoda, Hokkitsu-machi, Shibukawa 377-8577, Japan. [13]Division of Hematology, Internal Medicine, Showa University Fujigaoka Hospital, 1-30, Fujigaoka, Aoba-ku, Yokohama-shi, Kanagawa 227-8501, Japan. [14]Department of Pathology, Teikyo University School of Medicine, 2-11-1 Kaga, Itabashi-ku, Tokyo 173-8605, Japan.

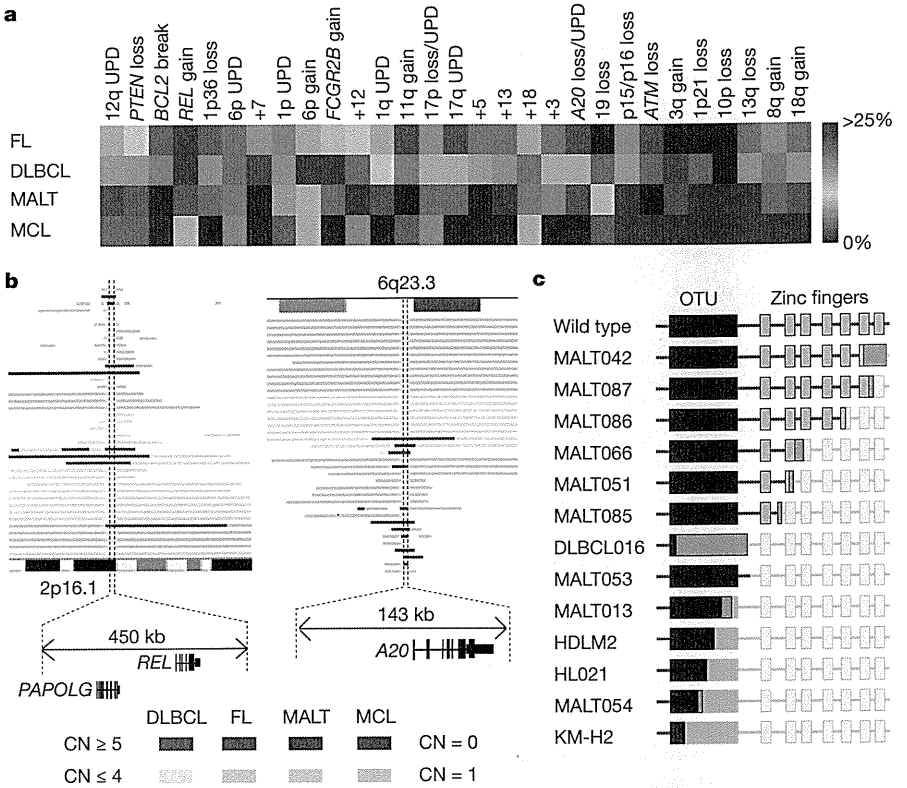

Figure 1 | Genomic signatures of different B-cell lymphomas and common genetic lesions at 2p16-15 and 6q23.3 involving NF-κB pathway genes. **a**, Twenty-nine genetic lesions were found in more than 10% in at least one histology and used for clustering four distinct histology types of B-lineage lymphomas. The frequency of each genetic lesion in each histology type is colour-coded. FL, follicular lymphoma; UPD, uniparental disomy. **b**, Recurrent genetic changes are depicted based on CNAG output of the SNP array analysis of 238 B-lineage lymphoma samples, which include gains at the *REL* locus on 2p16-15 (left panel) and the *A20* locus on 6q23.3 (right panel). Regions showing copy number gain or loss are indicated by horizontal lines. Four histology types are indicated by different colours, where high-grade amplifications and homozygous deletions are shown by darker shades to discriminate from simple gains (copy number ≤4) and losses (copy number = 1) (lighter shades). **c**, Point mutations and small nucleotide insertions and deletions in the *A20* (*TNFAIP3*) gene caused premature truncation of A20 in most cases. Altered amino acids caused by frame shifts are indicated by green bars.

genomic DNA was extracted from 150 microdissected CD30-positive tumour cells (Reed–Sternberg cells) for each sample. *A20* mutations were found in 18 out of 265 lymphoma samples (6.8%) (Table 1), among which 13 mutations, including nonsense mutations (3 cases), frame-shift insertions/deletions (9 cases), and a splicing donor site mutation (1 case) were thought to result in premature termination of translation (Fig. 1c). Four missense mutations and one intronic mutation were identified in five microdissected Hodgkin's lymphoma samples. They were not found in the surrounding normal tissues, and thus, were considered as tumour-specific somatic changes.

In total, biallelic *A20* lesions were found in 31 out of 265 lymphoma samples including 3 Hodgkin's lymphoma cell lines. Quantitative analysis of SNP array data suggested that these *A20* lesions were present in the major tumour fraction within the samples (Supplementary Fig. 7). Inactivation of *A20* was most frequent in MALT lymphoma (18 out of 87) and Hodgkin's lymphoma (7 out of 27), although it was also found in DLBCL (5 out of 64) and follicular lymphoma (1 out of 52) at lower frequencies. In MALT lymphoma, biallelic *A20* lesions were confirmed in 18 out of 24 cases (75.0%) with LOH involving the 6q23.3 segment (Supplementary Fig. 8). Considering the limitation in detecting very small homozygous deletions, *A20* was thought to be the target of 6q23 LOH in MALT lymphoma. On the other hand, the 6q23 LOHs in other histology types tended to be extended into more centromeric regions and less frequently accompanied biallelic *A20* lesions (Supplementary Fig. 8 and Supplementary Table 4), indicating that they might be more heterogeneous with regard to their gene targets. We were unable to analyse Hodgkin's lymphoma samples using SNP arrays owing to insufficient genomic DNA obtained from microdissected samples, and were likely to underestimate the frequency of *A20* inactivation in Hodgkin's lymphoma because we might fail to detect a substantial proportion of cases with homozygous deletions, which explained 50% (12 out of 24) of *A20* inactivation in other histology types. *A20* mutations in Hodgkin's lymphoma were exclusively found in nodular sclerosis classical Hodgkin's lymphoma (5 out of 15) but not in other histology types (0 out of 9), although the possible association requires further confirmation in additional cases.

A20 is a key regulator of NF-κB signalling, negatively modulating NF-κB activation through a wide variety of cell surface receptors and viral proteins, including tumour-necrosis factor (TNF) receptors, toll-like receptors, CD40, as well as Epstein–Barr-virus-associated LMP1 protein[2,5,17,18]. To investigate the role of A20 inactivation in lymphomagenesis, we re-expressed wild-type A20 under a *Tet*-inducible promoter in a lymphoma-derived cell line (KM-H2) that had no functional *A20* alleles (Supplementary Fig. 6), and examined the effect of A20 re-expression on cell proliferation, survival and downstream NF-κB signalling pathways. As shown in Fig. 2a–c and Supplementary Fig. 9, re-expression of wild-type A20 resulted in the suppression of cell proliferation and enhanced apoptosis, and in the concomitant accumulation of IκBβ and IκBε, and downregulation of NF-κB activity. In contrast, re-expression of two lymphoma-derived A20 mutants, $A20^{532Stop}$ or $A20^{750Stop}$, failed to show growth suppression, induction of apoptosis, accumulation of IκBβ and IκBε or downregulation of

Table 1 | Inactivation of A20 in B-lineage lymphomas

Histology	Tissue	Sample	Allele	Uniparental disomy	Exon	Mutation	Biallelic inactivation
DLBCL							5 out of 64 (7.8%)
	Lymph node	DLBCL008	−/−	No	–	–	
	Lymph node	DLBCL016	+/−	No	Ex2	329insA	
	Lymph node	DLBCL022	−/−	No	–	–	
	Lymph node	DLBCL028	−/−	Yes	–	–	
	Lymph node	MCL008*	−/−	Yes	–	–	
Follicular lymphoma							1 out of 52 (1.9%)
	Lymph node	FL024	−/−	No	–	–	
MCL							0 out of 35 (0%)
MALT							18 out of 87 (21.8%)
Stomach							3 out of 23 (13.0%)
	Gastric mucosa	MALT013	+/+	Yes	Ex5	705insG	
	Gastric mucosa	MALT014	+/+	Yes	Ex3	Ex3 donor site>A	
	Gastric mucosa	MALT036	+/−	No	Ex7	delintron6–Ex7†	
Eye							13 out of 43 (30.2%)
	Ocular adnexa	MALT008	−/−	No	–	–	
	Ocular adnexa	MALT017	−/−	No	–	–	
	Ocular adnexa	MALT051	+/−	No	Ex7	1943delTG	
	Ocular adnexa	MALT053	+/+	Yes	Ex6	1016G>A(stop)	
	Ocular adnexa	MALT054	+/−	No	Ex3	502delTC	
	Ocular adnexa	MALT055	−/−	No	–	–	
	Ocular adnexa	MALT066	+/−	No	Ex7	1581insA	
	Ocular adnexa	MALT067	−/−	No	–	–	
	Ocular adnexa	MALT082	−/−	Yes	–	–	
	Ocular adnexa	MALT084	−/−	Yes	–	–	
	Ocular adnexa	MALT085	+/+	Yes	Ex7	1435insG	
	Ocular adnexa	MALT086	+/+	Yes	Ex6	878C>T(stop)	
	Ocular adnexa	MALT087	+/+	Yes	Ex9	2304delGG	
Lung							2 out of 12 (16.7%)
	Lung	MALT042	−/−	No	–	–	
	Lung	MALT047	+/+	Yes	Ex9	2281insT	
Other‡							0 out of 9 (0%)
Hodgkin's lymphoma							7 out of 27 (26.0%)
NSHL	Lymph node	HL10	ND	ND	Ex7	1777G>A(V571I)	
NSHL	Lymph node	HL12	ND	ND	Ex7	1156A>G(R364G)	
NSHL	Lymph node	HL21	ND	ND	Ex4	569G>A(stop)	
NSHL	Lymph node	HL24	ND	ND	Ex3	1487C>A(T474N)	
NSHL	Lymph node	HL23	ND	ND	–	Intron 3§	
	Cell line	KM-H2	−/−	No	–		
	Cell line	HDLM2	+/−	No	Ex4	616ins29bp‖	
Total							31 out of 265 (11.7%)

DLBCL, diffuse large B-cell lymphoma; MALT, MALT lymphoma; MCL, mantle cell lymphoma; ND, not determined because SNP array analysis was not performed; NSHL, nodular sclerosis classical Hodgkin's lymphoma.
* Diagnosis was changed based on the genomic data, which was confirmed by re-examination of pathology.
† Deletion including the boundary of intron 6 and exon 7 (see also Supplementary Fig. 5b).
‡ Including 1 parotid gland, 1 salivary gland, 2 colon and 5 thyroid cases.
§ Insertion of CTC at −19 bases from the beginning of exon 3.
‖ Insertion of TGGCTTCCACAGACACACCCATGGCCCGA.

NF-κB activity (Fig. 2a–c), indicating that these were actually loss-of-function mutations. To investigate the role of A20 inactivation in lymphomagenesis *in vivo*, *A20*- and mock-transduced KM-H2 cells were transplanted in NOD/SCID/γ_c^{null} (NOG) mice[19], and their tumour formation status was examined for 5 weeks with or without induction of wild-type A20 by tetracycline administration. As shown in Fig. 2d, mock-transduced cells developed tumours at the injected sites, whereas the *Tet*-inducible *A20*-transduced cells generated tumours only in the absence of A20 induction (Supplementary Table 5), further supporting the tumour suppressor role of A20 in lymphoma development.

Given the mode of negative regulation of NF-κB signalling, we next investigated the origins of NF-κB activity that was deregulated by A20 loss in KM-H2 cells. The conditioned medium prepared from a 48-h serum-free KM-H2 culture had increased NF-κB upregulatory activity compared with fresh serum-free medium, which was inhibited by re-expression of A20 (Fig. 3a). KM-H2 cells secreted two known ligands for TNF receptor—TNF-α and lymphotoxin-α (Supplementary Fig. 10)[20]—and adding neutralizing antibodies against these cytokines into cultures significantly suppressed their cell growth and NF-κB activity without affecting the levels of their overall suppression after A20 induction (Fig. 3b, d). In addition, recombinant TNF-α and/or lymphotoxin-α added to fresh serum-free medium promoted cell growth and NF-κB activation in KM-H2 culture, which were again suppressed by re-expression of A20 (Fig. 3c, e). Although our data in Fig. 3 also show the presence of factors other than TNF-α and lymphotoxin-α in the KM-H2-conditioned medium—as well as some intrinsic pathways in the cell (Fig. 3a)—that were responsible for the A20-dependent NF-κB activation, these results indicate that both cell growth and NF-κB activity that were upregulated by A20 inactivation depend at least partly on the upstream stimuli that evoked the NF-κB-activating signals.

Aberrant activation of the NF-κB pathway is a hallmark of several subtypes of B-lineage lymphomas, including Hodgkin's lymphoma, MALT lymphoma, and a subset of DLBCL, as well as other lymphoid neoplasms[11,14], where a number of genetic alterations of NF-κB signalling pathway genes[21–25], as well as some viral proteins[26,27], have been implicated in the aberrant activation of the NF-κB pathway[14]. Thus, frequent inactivation of A20 in Hodgkin's lymphoma and MALT and other lymphomas provides a novel insight into the molecular pathogenesis of these subtypes of B-lineage lymphomas through deregulated NF-κB activation. Because A20 provides a

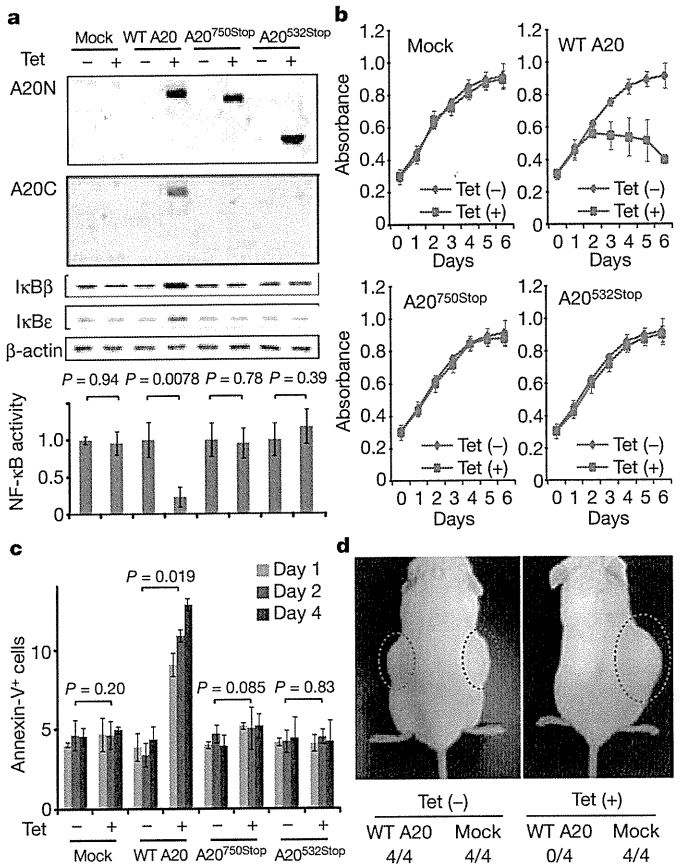

Figure 2 | Effects of wild-type and mutant A20 re-expressed in a lymphoma cell line that lacks the normal *A20* gene. a, Western blot analyses of wild-type (WT) and mutant ($A20^{532Stop}$ and $A20^{750Stop}$) A20, as well as IκBβ and IκBε, in KM-H2 cells, in the presence or absence of tetracycline treatment (top panels). A20N and A20C are polyclonal antisera raised against N-terminal and C-terminal A20 peptides, respectively. β-actin blots are provided as a control. NF-κB activities are expressed as mean absorbance ± s.d. ($n = 6$) in luciferase assays (bottom panel). **b,** Proliferation of KM-H2 cells stably transduced with plasmids for mock and *Tet*-inducible wild-type A20, $A20^{532Stop}$ and $A20^{750Stop}$ was measured using a cell counting kit in the presence (red lines) or absence (blue lines) of tetracycline. Mean absorbance ± s.d. ($n = 5$) is plotted. **c,** The fractions of Annexin-V-positive KM-H2 cells transduced with various *Tet*-inducible A20 constructs were measured by flow cytometry after tetracycline treatment and the mean values (±s.d., $n = 3$) are plotted. **d,** *In vivo* tumorigenicity was assayed by inoculating 7×10^6 KM-H2 cells transduced with mock or *Tet*-inducible wild-type A20 in NOG mice, with (right panel) or without (left panel) tetracycline administration.

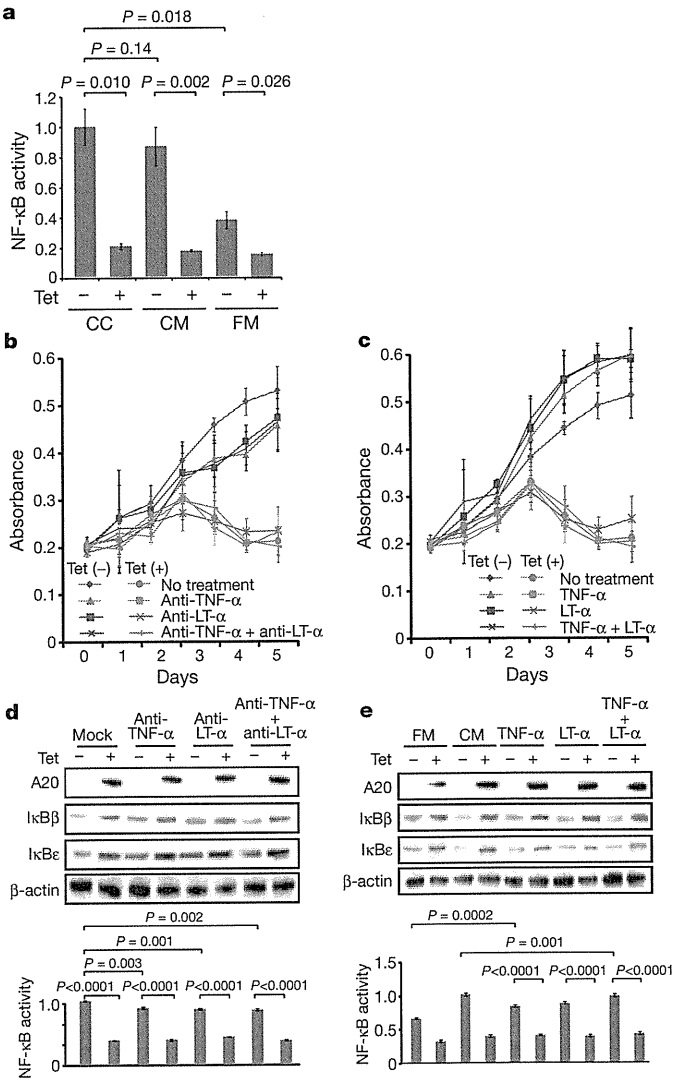

Figure 3 | Tumour suppressor role of A20 under external stimuli. a, NF-κB activity in KM-H2 cells was measured 30 min after cells were inoculated into fresh medium (FM) or KM-H2-conditioned medium (CM) obtained from the 48-h culture of KM-H2, and was compared with the activity after 48 h continuous culture of KM-H2 (CC). A20 was induced 12 h before inoculation in Tet (+) groups. **b, c,** Effects of neutralizing antibodies against TNF-α and lymphotoxin-α (LTα) (**b**) and of recombinant TNF-α and LT-α added to the culture (**c**) on cell growth were evaluated in the presence (Tet (+)) or absence (Tet (−)) of A20 induction. Cell numbers were measured using a cell counting kit and are plotted as their mean absorbance ± s.d. ($n = 6$). **d, e,** Effects of the neutralizing antibodies (**d**) and the recombinant cytokines added to the culture (**e**) on NF-κB activities and the levels of IκBβ and IκBε after 48 h culture with (Tet (+)) or without (Tet (−)) tetracycline treatment. NF-κB activities are expressed as mean absorbance ± s.d. ($n = 6$) in luciferase assays.

negative feedback mechanism in the regulation of NF-κB signalling pathways upon a variety of stimuli, aberrant activation of NF-κB will be a logical consequence of A20 inactivation. However, there is also the possibility that the aberrant NF-κB activity of A20-inactivated lymphoma cells is derived from upstream stimuli, which may be from the cellular environment. In this context, it is intriguing that MALT lymphoma usually arises at the site of chronic inflammation caused by infection or autoimmune disorders and may show spontaneous regression after eradication of infectious organisms[28]; furthermore, Hodgkin's lymphoma frequently shows deregulated cytokine production from Reed–Sternberg cells and/or surrounding reactive cells[29]. Detailed characterization of the NF-κB pathway regulated by A20 in both normal and neoplastic B lymphocytes will promote our understanding of the precise roles of A20 inactivation in the pathogenesis of these lymphoma types. Our finding underscores the importance of genome-wide approaches in the identification of genetic targets in human cancers.

METHODS SUMMARY

Genomic DNA from 238 patients with non-Hodgkin's lymphoma and three Hodgkin's-lymphoma-derived cell lines was analysed using GeneChip SNP genotyping microarrays (Affymetrix). This study was approved by the ethics boards of the University of Tokyo, National Cancer Institute Hospital, Okayama University, and the Cancer Institute of the Japanese Foundation of Cancer Research. After appropriate normalization of mean array intensities, signal ratios between tumours and anonymous normal references were calculated in an allele-specific manner, and allele-specific copy numbers were inferred from the observed signal ratios based on the hidden Markov model using CNAG/AsCNAR software (http://www.genome.umin.jp). *A20* mutations were examined by directly sequencing genomic DNA using a set of primers (Supplementary Table 6). Full-length cDNAs of wild-type and mutant *A20* were introduced into a

lentivirus vector, pLenti4/TO/V5-DEST (Invitrogen), with a *Tet*-inducible promoter. Viral stocks were prepared by transfecting the vector plasmids into 293FT cells (Invitrogen) using the calcium phosphate method and then infected to the KM-H2 cell line. Proliferation of KM-H2 cells was measured using a Cell Counting Kit (Dojindo). Western blot analyses and luciferase assays were performed as previously described. NF-κB activity was measured by luciferase assays in KM-H2 cells stably transduced with a reporter plasmid having an NF-κB response element, pGL4.32 (Promega). Apoptosis of KM-H2 upon A20 induction was evaluated by counting Annexin-V-positive cells by flow cytometry. For *in vivo* tumorigenicity assays, 7×10^6 KM-H2 cells were transduced with the *Tet*-inducible *A20* gene and those with a mock vector were inoculated on the contralateral sides in eight NOG mice[19] and examined for their tumour formation with ($n = 4$) or without ($n = 4$) tetracycline administration. Full copy number data of the 238 lymphoma samples will be accessible from the Gene Expression Omnibus (GEO, http://ncbi.nlm.nih.gov/geo/) with the accession number GSE12906.

Full Methods and any associated references are available in the online version of the paper at www.nature.com/nature.

Received 17 September 2008; accepted 3 March 2009.
Published online 3 May 2009.

1. Dixit, V. M. *et al.* Tumor necrosis factor-α induction of novel gene products in human endothelial cells including a macrophage-specific chemotaxin. *J. Biol. Chem.* **265**, 2973–2978 (1990).
2. Song, H. Y., Rothe, M. & Goeddel, D. V. The tumor necrosis factor-inducible zinc finger protein A20 interacts with TRAF1/TRAF2 and inhibits NF-κB activation. *Proc. Natl Acad. Sci. USA* **93**, 6721–6725 (1996).
3. Lee, E. G. *et al.* Failure to regulate TNF-induced NF-κB and cell death responses in A20-deficient mice. *Science* **289**, 2350–2354 (2000).
4. Boone, D. L. *et al.* The ubiquitin-modifying enzyme A20 is required for termination of Toll-like receptor responses. *Nature Immunol.* **5**, 1052–1060 (2004).
5. Wang, Y. Y., Li, L., Han, K. J., Zhai, Z. & Shu, H. B. A20 is a potent inhibitor of TLR3- and Sendai virus-induced activation of NF-κB and ISRE and IFN-β promoter. *FEBS Lett.* **576**, 86–90 (2004).
6. Wertz, I. E. *et al.* De-ubiquitination and ubiquitin ligase domains of A20 downregulate NF-κB signalling. *Nature* **430**, 694–699 (2004).
7. Heyninck, K. & Beyaert, R. A20 inhibits NF-κB activation by dual ubiquitin-editing functions. *Trends Biochem. Sci.* **30**, 1–4 (2005).
8. Graham, R. R. *et al.* Genetic variants near *TNFAIP3* on 6q23 are associated with systemic lupus erythematosus. *Nature Genet.* **40**, 1059–1061 (2008).
9. Musone, S. L. *et al.* Multiple polymorphisms in the *TNFAIP3* region are independently associated with systemic lupus erythematosus. *Nature Genet.* **40**, 1062–1064 (2008).
10. Jaffe, E. S., Harris, N. L., Stein, H. & Vardiman, J. W. *World Health Organization Classification of Tumours. Pathology and Genetics of Tumours of Hematopoietic and Lymphoid Tissues* (IARC Press, 2001).
11. Klein, U. & Dalla-Favera, R. Germinal centres: role in B-cell physiology and malignancy. *Nature Rev. Immunol.* **8**, 22–33 (2008).
12. Nannya, Y. *et al.* A robust algorithm for copy number detection using high-density oligonucleotide single nucleotide polymorphism genotyping arrays. *Cancer Res.* **65**, 6071–6079 (2005).
13. Yamamoto, G. *et al.* Highly sensitive method for genomewide detection of allelic composition in nonpaired, primary tumor specimens by use of affymetrix single-nucleotide-polymorphism genotyping microarrays. *Am. J. Hum. Genet.* **81**, 114–126 (2007).
14. Jost, P. J. & Ruland, J. Aberrant NF-κB signaling in lymphoma: mechanisms, consequences, and therapeutic implications. *Blood* **109**, 2700–2707 (2007).
15. Durkop, H., Hirsch, B., Hahn, C., Foss, H. D. & Stein, H. Differential expression and function of A20 and TRAF1 in Hodgkin lymphoma and anaplastic large cell lymphoma and their induction by CD30 stimulation. *J. Pathol.* **200**, 229–239 (2003).
16. Honma, K. *et al. TNFAIP3* is the target gene of chromosome band 6q23.3-q24.1 loss in ocular adnexal marginal zone B cell lymphoma. *Genes Chromosom. Cancer* **47**, 1–7 (2008).
17. Sarma, V. *et al.* Activation of the B-cell surface receptor CD40 induces A20, a novel zinc finger protein that inhibits apoptosis. *J. Biol. Chem.* **270**, 12343–12346 (1995).
18. Fries, K. L., Miller, W. E. & Raab-Traub, N. The A20 protein interacts with the Epstein-Barr virus latent membrane protein 1 (LMP1) and alters the LMP1/TRAF1/TRADD complex. *Virology* **264**, 159–166 (1999).
19. Hiramatsu, H. *et al.* Complete reconstitution of human lymphocytes from cord blood $CD34^+$ cells using the NOD/SCID/γ^{null} mice model. *Blood* **102**, 873–880 (2003).
20. Hsu, P. L. & Hsu, S. M. Production of tumor necrosis factor-α and lymphotoxin by cells of Hodgkin's neoplastic cell lines HDLM-1 and KM-H2. *Am. J. Pathol.* **135**, 735–745 (1989).
21. Dierlamm, J. *et al.* The apoptosis inhibitor gene *API2* and a novel 18q gene, *MLT*, are recurrently rearranged in the t(11;18)(q21;q21) associated with mucosa-associated lymphoid tissue lymphomas. *Blood* **93**, 3601–3609 (1999).
22. Willis, T. G. *et al.* Bcl10 is involved in t(1;14)(p22;q32) of MALT B cell lymphoma and mutated in multiple tumor types. *Cell* **96**, 35–45 (1999).
23. Joos, S. *et al.* Classical Hodgkin lymphoma is characterized by recurrent copy number gains of the short arm of chromosome 2. *Blood* **99**, 1381–1387 (2002).
24. Martin-Subero, J. I. *et al.* Recurrent involvement of the *REL* and *BCL11A* loci in classical Hodgkin lymphoma. *Blood* **99**, 1474–1477 (2002).
25. Lenz, G. *et al.* Oncogenic *CARD11* mutations in human diffuse large B cell lymphoma. *Science* **319**, 1676–1679 (2008).
26. Deacon, E. M. *et al.* Epstein-Barr virus and Hodgkin's disease: transcriptional analysis of virus latency in the malignant cells. *J. Exp. Med.* **177**, 339–349 (1993).
27. Yin, M. J. *et al.* HTLV-I Tax protein binds to MEKK1 to stimulate IκB kinase activity and NF-κB activation. *Cell* **93**, 875–884 (1998).
28. Isaacson, P. G. & Du, M. Q. MALT lymphoma: from morphology to molecules. *Nature Rev. Cancer* **4**, 644–653 (2004).
29. Skinnider, B. F. & Mak, T. W. The role of cytokines in classical Hodgkin lymphoma. *Blood* **99**, 4283–4297 (2002).

Supplementary Information is linked to the online version of the paper at www.nature.com/nature.

Acknowledgements This work was supported by the Core Research for Evolutional Science and Technology, Japan Science and Technology Agency, by the 21st century centre of excellence program 'Study on diseases caused by environment/genome interactions', and by Grant-in-Aids from the Ministry of Education, Culture, Sports, Science and Technology of Japan and from the Ministry of Health, Labor and Welfare of Japan for the 3rd-term Comprehensive 10-year Strategy for Cancer Control. We also thank Y. Ogino, E. Matsui and M. Matsumura for their technical assistance.

Author Contributions M.Ka., K.N. and M.S. performed microarray experiments and subsequent data analyses. M.Ka., Y.C., K.Ta., J.T., J.N., M.I., A.T. and Y.K. performed mutation analysis of *A20*. M.Ka., S.Mu., M.S., Y.C. and Y.Ak. conducted functional assays of mutant A20. Y.S., K.Ta., Y.As., H.M., M.Ku., S.Mo., S.C., Y.K., K.To. and Y.I. prepared tumour specimens. I.K., K.O., A.N., H.N. and T.N. conducted *in vivo* tumorigenicity experiments in NOG/SCID mice. T.I., Y.H., T.Y., Y.K. and S.O. designed overall studies, and S.O. wrote the manuscript. All authors discussed the results and commented on the manuscript.

Author Information The copy number data as well as the raw microarray data will be accessible from the GEO (http://ncbi.nlm.nih.gov/geo/) with the accession number GSE12906. Reprints and permissions information is available at www.nature.com/reprints. Correspondence and requests for materials should be addressed to S.O. (sogawa-tky@umin.ac.jp) or Y.K. (ykkobaya@ncc.go.jp).

METHODS

Specimens. Primary tumour specimens were obtained from patients who were diagnosed with DLBCL, follicular lymphoma, MCL, MALT lymphoma, or classical Hodgkin's lymphoma. In total, 238 primary lymphoma specimens listed in Supplementary Table 1 were subjected to SNP array analysis. Three Hodgkin's-lymphoma-derived cell lines (KM-H2, HDLM2, L540) were obtained from Hayashibara Biochemical Laboratories, Inc., Fujisaki Cell Center and were also analysed by SNP array analysis.

Microarray analysis. High-molecular-mass DNA was isolated from tumour specimens and subjected to SNP array analysis using GeneChip Mapping 50K and/or 250K arrays (Affymetrix). The scanned array images were processed with Gene Chip Operation software (GCOS), followed by SNP calls using GTYPE. Genome-wide copy number measurements and LOH detection were performed using CNAG/AsCNAR software[12,13].

Mutation analysis. Mutations in the *A20* gene were examined in 265 samples of B-lineage lymphoma, including 62 DLBCLs, 52 follicular lymphomas, 87 MALTs, 37 MCLs and 3 Hodgkin's-lymphoma-derived cell lines and 24 primary Hodgkin's lymphoma samples, by direct sequencing using an ABI PRISM 3130xl Genetic Analyser (Applied Biosystems). To analyse primary Hodgkin's lymphoma samples in which CD30-positive tumour cells (Reed–Sternberg cells) account for only a fraction of the specimen, 150 Reed–Sternberg cells were collected for each 10 μm slice of a formalin-fixed block immunostained for CD30 by laser-capture microdissection (ASLMD6000, Leica), followed by genomic DNA extraction using QIAamp DNA Micro kit (Qiagen). The primer sets used in this study are listed in Supplementary Table 6.

Functional analysis of wild-type and mutant A20. Full-length cDNA for wild-type *A20* was isolated from total RNA extracted from an acute myeloid leukaemia-derived cell line, CTS, and subcloned into a lentivirus vector (pLenti4/TO/V5-DEST, Invitrogen). cDNAs for mutant A20 were generated by PCR amplification using mutagenic primers (Supplementary Table 6), and introduced into the same lentivirus vector. Forty-eight hours after transfection of each plasmid into 293FT cells using the calcium phosphate method, lentivirus stocks were obtained from ultrafiltration using Amicon Ultra (Millipore), and used to infect KM-H2 cells to generate stable transfectants of mock, wild-type and mutant A20. Each KM-H2 derivative cell line was further transduced stably with a reporter plasmid (pGL4.32, Promega) containing a luciferase gene under an NF-κB-responsive element by electroporation using Nucleofector reagents (Amaxa).

Assays for cell proliferation and NF-κB activity. Proliferation of the KM-H2 derivative cell lines was assayed in triplicate using a Cell Counting Kit (Dojindo). The mean absorption of five independent assays was plotted with s.d. for each derivative line. Two independent KM-H2-derived cell lines were used for each experiment. The NF-κB activity in KM-H2 derivatives for A20 mutants was evaluated by luciferase assays using a PiccaGene Luciferase Assay Kit (TOYO B-Net Co.). Each assay was performed in triplicate and the mean absorption of five independent experiments was plotted with s.d.

Western blot analyses. Polyclonal anti-sera against N-terminal (anti-A20N) and C-terminal (anti-A20C) A20 peptides were generated by immunizing rabbits with these peptides (LSNMRKAVKIRERTPEDIC for anti-A20N and CFQFKQMYG for anti-A20C, respectively). Total cell lysates from KM-H2 cells were separated on 7.5% polyacrylamide gel and subjected to western blot analysis using antibodies to A20 (anti-A20N and anti-A20C), IκBα (sc-847), IκBβ (sc-945), IκBγ (sc-7155) and actin (sc-8432) (Santa Cruz Biotechnology).

Functional analyses of wild-type and mutant A20. Each KM-H2 derivative cell line stably transduced with various *Tet*-inducible A20 constructs was cultured in serum-free medium in the presence or absence of A20 induction using 1 μg ml^{-1} of tetracycline, and cell number was counted every day. 1×10^6 cells of each KM-H2 derivative cell line were analysed for their intracellular levels of IκBβ and IκBε and for NF-κB activities by western blot analyses and luciferase assays, respectively, 12 h after the beginning of cell culture. Effects of human recombinant TNF-α and lymphotoxin-α (210-TA and 211-TB, respectively, R&D Systems) on the NF-κB pathway and cell proliferation were evaluated by adding both cytokines into 10 ml of serum-free cell culture at a concentration of 200 pg ml^{-1}. For cell proliferation assays, culture medium was half replaced every 12 h to minimize the side-effects of autocrine cytokines. Intracellular levels of IκBβ, IκBε and NF-κB were examined 12 h after the beginning of the cell culture. To evaluate the effect of neutralizing TNF-α and lymphotoxin-α, 1×10^6 of KM-H2 cells transduced with both *Tet*-inducible A20 and the NF-κB-luciferase reporter were pre-cultured in serum-free media for 36 h, and thereafter neutralizing antibodies against TNF-α (MAB210, R&D Systems) and/or lymphotoxin-α (AF-211-NA, R&D Systems) were added to the media at a concentration of 200 pg ml^{-1}. After the extended culture during 12 h with or without 1 μg ml^{-1} tetracycline, the intracellular levels of IκBβ and IκBε and NF-κB activities were examined by western blot analysis and luciferase assays, respectively. To examine the effects of A20 re-expression on apoptosis, 1×10^6 KM-H2 cells were cultured for 4 days in 10 ml medium with or without *Tet* induction. After staining with phycoerythrin-conjugated anti-Annexin-V (ID556422, Becton Dickinson), Annexin-V-positive cells were counted by flow cytometry at the indicated times.

***In vivo* tumorigenicity assays.** KM-H2 cells transduced with a mock or *Tet*-inducible wild-type *A20* gene were inoculated into NOG mice and their tumorigenicity was examined for 5 weeks with or without tetracycline administration. Injections of 7×10^6 cells of each KM-H2 cell line were administered to two opposite sites in four mice. Tetracycline was administered in drinking water at a concentration of 200 μg ml^{-1}.

ELISA. Concentrations of TNF-α, lymphotoxin-α, IL-1, IL-2, IL-4, IL-6, IL-12, IL-18 and TGF-β in the culture medium were measured after 48 h using ELISA. For those cytokines detectable after 48-h culture (TNFα, LTα, and IL-6), their time course was examined further using the Quantikine ELISA kit (R&D Systems).

Statistical analysis. Significance of the difference in NF-κB activity between two given groups was evaluated using a paired *t*-test, in which the data from each independent luciferase assay were paired to calculate test statistics. To evaluate the effect of A20 re-expression in KM-H2 cells on apoptosis, the difference in the fractions of Annexin-V-positive cells between Tet (+) and Tet (−) groups was also tested by a paired *t*-test for assays, in which the data from the assays performed on the same day were paired.

Modern Pathology (2009) 22, 508–515
 0893-3952/09 $32.00
www.modernpathology.org

EML4-ALK lung cancers are characterized by rare other mutations, a TTF-1 cell lineage, an acinar histology, and young onset

Kentaro Inamura[1,4], Kengo Takeuchi[1,4], Yuki Togashi[1], Satoko Hatano[1], Hironori Ninomiya[1], Noriko Motoi[1], Ming-yon Mun[2], Yukinori Sakao[2], Sakae Okumura[2], Ken Nakagawa[2], Manabu Soda[3], Young Lim Choi[3], Hiroyuki Mano[3] and Yuichi Ishikawa[1]

[1]*Division of Pathology, The Cancer Institute, Japanese Foundation for Cancer Research (JFCR), Koto-ku, Tokyo, Japan;* [2]*Department of Thoracic Surgery, The Cancer Institute Hospital, Japanese Foundation for Cancer Research (JFCR), Koto-ku, Tokyo, Japan and* [3]*Division of Functional Genomics, Jichi Medical University, Tochigi, Japan*

A subset of lung cancers harbors a small inversion within chromosome 2p, giving rise to a transforming fusion gene, *EML4-ALK* (*echinoderm microtubule-associated protein-like 4 gene* and the *anaplastic lymphoma kinase gene*), which encodes an activated tyrosine kinase. We have earlier examined the presence of *EML4-ALK* by multiplex reverse transcription-polymerase chain reaction in 363 specimens of lung cancer, identifying 11 adenocarcinoma cases featuring the fusion gene. In this study, we clinicopathologically examined the characteristics of the *EML4-ALK*-positive cases, including the mutation status of *EGFR*, *KRAS*, and *TP53*, and whether they were of thyroid transcription factor-1 (TTF-1) cell lineage or not. Of 11 patients, 4 (36%) with *EML4-ALK*-positive lung adenocarcinomas who were below 50 years of age were affected by these diseases, as compared with 12 of 242 patients (5.0%) with *EML4-ALK*-negative lung adenocarcinomas ($P=0.00038$). *EML4-ALK*-positive lung adenocarcinomas were characterized by less-differentiated grade ($P=0.0082$) and acinar-predominant structure ($P<0.0001$) in histology. Furthermore, the presence of *EML4-ALK* appears to be mutually exclusive for *EGFR* and *KRAS* mutations ($P=0.00018$), whereas coexisting with *TP53* mutations at a low frequency (1/11 = 9.1%), and correlating with non- or light smoking ($P=0.040$), in line with the TTF-1 immunoreactivity. Thus, *EML4-ALK*-positive tumors may form a distinct entity among lung adenocarcinomas, characterized by young onset, acinar histology, no or rare mutations in *EGFR*, *KRAS*, and *TP53*, and a TTF-1 cell lineage, all in agreement with the prevalence in non- or light smokers.
Modern Pathology (2009) **22,** 508–515; doi:10.1038/modpathol.2009.2; published online 20 February 2009

Keywords: lung cancer; *EML4-ALK*; gene mutation; TTF-1; histology

Lung cancer is one of the leading causes of cancer death in both men and women worldwide. Activating mutations within *epidermal growth factor receptor* (*EGFR*) have been identified in lung cancers,[1,2] and chemical inhibitors for the kinase activity of EGFR have been found effective in treatment of a subset of lung cancer patients harboring such mutations. Interestingly, the tumors for which EGFR inhibitors are effective develop preferentially in populations of Asian ethnicity and non-smokers, and generally lack *KRAS* mutations.[2–4] Furthermore, such tumors have low rates of smoking-specific *TP53* mutations, such as G/C to T/A transversions.[5,6]

Recently, we have found a novel transforming fusion gene joining the *echinoderm microtubule-associated protein-like 4 gene* (*EML4*) and the *anaplastic lymphoma kinase gene* (*ALK*) in four lung adenocarcinomas and one squamous cell carcinoma.[7] The *EML4-ALK* fusion gene is formed by a small inversion within chromosome 2p. The encoded protein contains the N-terminal part of *EML4* and the intracellular catalytic domain of *ALK*. Replacement of the extracellular and transmembrane domain of ALK with a region of EML4 results in constitutive dimerization of the kinase domain and thereby a consequent increase in its catalytic activity.[7]

Correspondence: Dr Y Ishikawa, Division of Pathology, The Cancer Institute, Japanese Foundation for Cancer Research, 3-10-6 Ariake, Koto-ku, Tokyo 135-8550, Japan.
E-mail: ishikawa@jfcr.or.jp
[4]These authors contributed equally to this work.
Received 07 October 2008; revised and accepted 8 December 2008; published online 20 February 2009

More recently, we have identified novel variants for *EML4-ALK* fusion gene with cDNA screening and multiplex reverse transcription-polymerase chain reaction (RT-PCR), capturing all possible in-frame fusions of *EML4* to exon 20 of *ALK*. By carrying out cDNA screening, we identified variant 3,[8] and using multiplex RT-PCR assays, we identified variants 4 and 5[9] after the first identification of variants 1 and 2. In variant 3, exon 6 of *EML4* is joined to exon 20 of *ALK*. cDNA from variant 4 ligates exon 14 of *EML4* to a position within exon 20 of *ALK*, whereas another cDNA from a variant 5 tumor connects exon 2 of *EML4* to exon 20 of *ALK*. All the new three isoforms of *EML4-ALK* have a marked oncogenic activity *in vitro* as well as *in vivo*.[8,9] The variant 3 was also identified by Rikova *et al*[10] and another new variant, in which exon 15 of *EML4* is jointed to a position within exon 20 of *ALK*, was identified by Koivunen *et al*.[11]

Earlier we conducted the first large scale-study to detect *EML4-ALK* (3.4%) in lung adenocarcinomas and found five fusion-positive cases (two variant 1 and three variant 2) in 149 adenocarcinoma samples.[12] At that point in time, only two variants were recognized, and we investigated their clinicopathological characteristics. However, with development of multiplex RT-PCR for detecting all possible in-frame variants, we captured theoretically all *EML4-ALK* variants and found 11 *EML4-ALK*-positive cases among 363 lung cancers.[9] In this study, we examined the clinicopathological and genetic features of the 11 tumors, and found *EML4-ALK* lung cancers to be characterized by a lack of *EGFR* and *KRAS* mutations, a low rate for *TP53* mutations, a thyroid transcription factor-1 (TTF-1)-positive cell lineage, an acinar histology, and young onset.

Materials and methods

Clinical Samples and Pathological Review

The clinical specimens for this study were 11 lung tumors detected in our earlier study, using multiplex RT-PCR and fluorescent *in situ* hybridization.[9] Briefly, samples were obtained from 363 individuals who underwent surgery at the Cancer Institute Hospital (Tokyo, Japan) between May 1997 and February 2004. The 363 lung cancers comprised 253 adenocarcinomas, 7 adenosquamous carcinomas, 72 squamous cell carcinomas, 7 large-cell carcinomas (including 4 large-cell neuroendocrine carcinomas), 2 pleomorphic carcinomas, and 22 small-cell carcinomas. This project was approved by the Institutional Review Board of the Japanese Foundation for Cancer Research, and informed consent was obtained from each study subject. Histological diagnoses were made based on the World Health Organization (WHO) classification.[13] However, with its subdivision of lung adenocarcinomas, more than 80% tumors fell into the mixed subtype category. We therefore additionally used a predominance classification of invasive components, which is mostly based on the WHO classification except for the mixed subtype, such as papillary predominant, acinar predominant, etc. In the predominance classification of invasive components, we diagnose by a component that makes up the predominant portion of invasive lesion even if it is <50%. In addition, we used a differentiation grading that was basically according to the former version of the Japanese Lung Cancer Society criteria,[14] as performed earlier.[15]

Immunohistochemical Analysis

Unstained paraffin-embedded sections were depleted of paraffin with xylene, rehydrated through a graded series of ethanol solutions, and subjected to immunohistochemical staining with a mouse monoclonal antibody (ALK1, 1:20, Dako, Carpinteria, CA, USA). Heat-induced antigen retrieval pretreatment was performed with Target Retrieval Solution pH 9.0 (Dako). Immune complexes were detected with the EnVision+DAB system (Dako) with minor modifications.[16] TTF-1 was also immunostained using a mouse monoclonal antibody (clone 8G7G3/1, 1:100, Dako), as described earlier.[15] Tumors were considered negative if staining was found in <5% of neoplastic cells, partly positive if present in 5–50%, and positive if in more than 50%. The results of immunostaining with TTF-1 were based on nuclear staining of neoplastic cells.

DNA Extraction and Mutation Analysis of *EGFR*, *KRAS*, and *TP53*

Of 253 patients with adenocarcinomas, both *EGFR* and *KRAS* data were available for 68 patients and *EGFR* data alone for further 12 patients, including all the patients with *EML4-ALK*-positve cases.[12,17] DNA extraction and mutation analysis of *EGFR* and *KRAS* were performed as described earlier.[17] Mutation analysis of *TP53* was also performed as described earlier.[18] Genomic DNAs from fresh tumor samples were prepared and exons 4–8 and 10 of the *TP53* gene were analyzed by the PCR – single-strand conformation polymorphism and DNA sequencing. For case #4808, *TP53* mutation analysis was performed using DNA extracted from formalin-fixed paraffin-embedded tissue and a method based on direct sequencing, because no fresh sample was available for this study at the time of the current study.

Results

Histologically, the 253 adenocarcinomas comprised 213 mixed subtypes, 19 acinar, 9 papillary, 4 solid, 1 other, and 7 bronchioloalveolar carcinomas based on the WHO classification. According to the subdivision

of lung adenocarcinomas with the WHO criteria, more than 80% of tumors fell into the mixed subtype category. However, this contains very varied lesions; for example, a tumor comprising solid and acinar adenocarcinoma elements would be expected to have a very different prognosis from one composed of bronchioloalveolar carcinoma, with only a small amount of papillary adenocarcinoma. We therefore additionally used a predominance classification and also paid attention to the minor components. According to the predominance subtypes in adenocarcinomas, 6 of 11 *EML4-ALK*-positive lung cancers (54.5%) were subclassified as acinar adenocarcinomas ($P=0.000044$, Table 1), as compared with 4 based on the WHO classification (36.4%, $P=0.0018$, Table 2). In other words, 6 of 34 (18%) acinar-predominant adenocarcinomas, as well as 4 of 19 (21%) acinar adenocarcinomas based on the WHO classification, have *EML4-ALK* fusion. In adenocarcinomas not subclassified as acinar adenocarcinomas based on the WHO criteria, acinar structures were also frequently observed (Figure 1). In differentiation grading, *EML4-ALK* lung cancers were less differentiated (Table 3, $P=0.0082$, 10/11). In addition, they often featured mucin production, as proven by Alcian Blue staining (Figure 1b) with acinar structures. As for the cell types originally proposed by Hashimoto *et al*,[18] the columnar cell type was characteristic of *EML4-ALK* lung cancers (Figure 1).

EML4-ALK-positive lung adenocarcinomas were also found to be significantly smaller than other lung adenocarcinomas (Table 3, $P=0.031$), in line with the lack of bronchioloalveolar components.

Patients with *EML4-ALK* lung cancers tended to be young (56 *vs* 64 years for other tumor types, $P=0.0062$). We defined early-onset lung cancers by classifying patients as below or above 50 years of age. In 253 patients with lung adenocarcinomas, 16 patients were affected by the disease at below 50 years of age. Four of 11 patients (36%) with *EML4-ALK*-positive lung cancers were affected by these diseases at below 50 years of age, as compared with 12 of 242 patients (5.0%) with *EML4-ALK*-negative lung cancers ($P=0.00038$).

It is true that the *EML4-ALK* translocation was first found in a smoker's lung cancer, but overall there was no significant difference between smokers' and non-smokers' tumors with regard to *EML4-ALK* fusion ($P=0.37$). Smoking habits can be classified into the following two grades of cumulative smoking based on the smoking index (SI), a product of the number of cigarettes per day, and the duration in years: (a) non-smokers and light smokers (SI <400); and (b) heavy smokers (SI $=400$ or above). Ten of the 11 (91%) *EML4-ALK*-positive lung cancer patients had SI <400, as compared with 109 of 241 (45%) *EML4-ALK*-negative lung cancer patients ($P=0.040$). In this study, *EML4-ALK* fusion was detected in only one heavy smoker's lung cancer (1/11 = 9.1%).

EGFR and *KRAS* mutations are mutually exclusive in usual cases while being two major oncogenic drivers of lung adenocarcinoma development. *EML4-ALK*-positive lung cancers lacked both *EGFR* and *KRAS* mutations ($P=0.00018$), and only 1 of 11 (9.1%) harbored a *TP53* mutation (Table 2). It is noteworthy that the single mutation was a G/A transition (GTG→ATG) (V→M) in codon 273, exon 8. This is known to be a spontaneous rather than a tobacco-carcinogen-induced mutation, usually seen in non-smokers' lung cancers.

In the *EML4-ALK*-positive 11 cases, immunohistochemical assays with the anti-ALK antibody ALK1 consistently showed definite staining. As illustrated

Table 1 *EML4-ALK* fusion and histology of adenocarcinomas classified by predominant subtypes

Histology	*Total (363)*	*EML4-ALK(+)*	*EML4-ALK(−)*
Adenocarcinoma	253	11 (4.3%)	242 (96%)
Subtype by predominance classification			
Invasive carcinoma			
Papillary adenocarcinoma	206	5 (5/11 = 45%)	201 (201/242 = 83%)
Acinar adenocarcinoma	34	6 (6/11 = 55%)[a]	28 (28/242 = 12%)
Solid adenocarcinoma with mucin	5	0 (0%)	5 (5/242 = 2.1%)
Others	1	0 (0%)	1 (1/242 = 0.41%)
Noninvasive carcinoma			
Bronchioloalveolar carcinoma	7	0 (0%)	7 (7/242 = 2.9%)
Adenosquamous carcinoma	7	0 (0%)	7 (100%)
Squamous cell carcinoma	72	0 (0%)	72 (100%)
Large-cell carcinoma	7	0 (0%)	7 (100%)
Large-cell neuroendocrine carcinoma	4	0 (0%)	4 (100%)
Pleomorphic carcinoma	2	0 (0%)	2 (100%)
Small-cell carcinoma	22	0 (0%)	22 (100%)

Acinar-predominant adenocarcinomas *vs* the other adenocarcinomas.
[a]Fisher's exact test, $P<0.0001$ ($P=0.000044$).

Table 2 *EML4-ALK* variants detected by multiplex RT-PCR analysis and clinicopathologic and genetic data

V	*Tumor ID*	*Sex*	*Age (years)*	*p-Stage*	*LKD*	*Survival (days)*	*Size (mm)*	*SI*	*WHO subtype*	*Pred-subtype*	*diff.*	*Histological components*	*ALK IHC*	*TTF-1 IHC*	*KRAS mut*	*EGFR mut*	*TP53 mut*
1	#9034	F	43	IA	Alive	1714	12	10	Acinar	Acinar	Por		+	P+	–	–	–
1	#4808	F	58	IA	Alive	2246	27	0	Mixed	Pap	Well	Papillary adenocarcinoma with BAC	+	+	–	–	–
1	#9968	F	66	IIIA	Alive	1036	33	0	Mixed	Pap	Mod	Papillary adenocarcinoma with BAC	+	+	–	–	–
2	#4180	M	43	IV	Dead	527	23	160	Acinar	Acinar	Por		+	P+	–	–	–
2	#3121	M	64	IIIB	Alive	2673	18	220	Acinar	Acinar	Por		+	+	–	–	–
2	#2374	F	66	IA	Alive	1632	28	0	Acinar	Acinar	Mod		+	P+	–	–	–
3	#7969	M	47	IIIA	Alive	1328	17	540	Mixed	Pap	Por	Papillary adenocarcinoma with BAC	+	+	–	–	–
3	#2075	F	62	IIA	Dead	522	19	0	Mixed	Acinar	Mod	Acinar+papillary+solid adenocarcinoma	+	P+	–	–	+[a]
3	#9616	M	73	IA	Alive	1465	13	300	Pap	Pap	Mod		+	+	–	–	–
4	#8398	F	52	IA	Alive	1834	24	0	Mixed	Acinar	Mod	Acinar+papillary adenocarcinoma with BAC	+	P+	–	–	–
5	#8993	M	44	IA	Alive	1730	15	0	Pap	Pap	Mod		+	+	–	–	–

acinar, acinar adenocarcinoma; BAC, bronchioloalveolar carcinoma; diff., differentiation; *EGFR* mut, *EGFR* mutation; IHC, immunohistochemistry; *KRAS* mut, *KRAS* mutation; LKD, lung cancer death; mixed, adenocarcinoma with mixed subtype; P+, Partly +; pap, papillary adenocarcinoma; Pred-subtype, predominance subtype; p-Stage, pathological-Stage; SI, smoking index; *TP53* mut, *TP53* mutation; V, *EML4-ALK* variant.

[a]G/A transition (GTG→ATG) (V→M) in codon 273, exon 8.

in Figure 2a, the cytoplasm of tumor cells harboring the variant 2 (tumor ID #2374) was strongly stained with fine granular accentuation. Although we performed the immunostaining of 88 *EML4-ALK*-negative lung adenocarcinoma specimens, we could discriminate all the fusion-negative specimens from the fusion-positive ones by our refined immunohistochemical condition.[16] All the 11 cases were also positive (six cases) or partly positive (five cases) for TTF-1 immunohistochemistry (Figure 2b), a characteristic of alveolar type II cells, which is featured in non-smokers' cancers.

Discussion

With the present large-scale screen for *EML4-ALK* fusion in lung cancers, we detected 11 adenocarcinomas with an *EML4-ALK* translocation. In the current study, we revealed a relatively young occurrence and a typically less-differentiated acinar histology, which might be used as clinical pointers. It is of great interest that *EML4-ALK* translocation is associated with young onset, whereas *EGFR* mutation status is not associated with the patient's age at diagnosis.[4]

Currently, anaplastic large-cell lymphomas (ALCLs) are divided into three entities, namely primary systemic *ALK* (+) ALCL, primary systemic *ALK* (−) ALCL, and primary cutaneous ALCL. The ALK expression is caused most commonly t(2;5) by chromosomal translocations, and *ALK* (+) ALCL predominantly affects young male patients and, if treated with chemotherapy, has a favorable prognosis.[19] This might similarly be applicable to *EML4-ALK* lung cancers. Presently, the primary treatment for lung cancers is surgery where possible. However, for *EML4-ALK* lung cancers, chemotherapy or a targeted therapy with an ALK inhibitor might be effective, given that *EML4-ALK*-dependent cells are known to undergo apoptosis in response.[7–9,11]

Here, *EML4-ALK* fusion was found to be mutually exclusive for *EGFR* or *KRAS* mutations, thus pointing to a distinct genetic subtype of lung adenocarcinoma. The possibility of a genetic classification of lung adenocarcinomas based on oncogene mutations has already been considered. In fact, one-third to nearly half of Japanese adenocarcinomas harbor *EGFR* mutations,[4,20] about 10% have *KRAS* mutations[21–23] and about 4% have *EML4-ALK* translocations, implying that two-thirds of adenocarcinomas feature mutually exclusive oncogenic mutations. The mutation rate of *TP53* (1/11 = 9.1%) was also low compared with that of lung adenocarcinomas in general (41%),[18] and the single mutation found was G to A transition, which was not related to smoking. Strong *in vitro* as well as *in vivo* oncogenic activity of *EML4-ALK* fusion products[8,9] might account for the lack of other genetic alterations.

All 11 *EML4-ALK* lung cancers were positive or partly positive for TTF-1 immunostaining. TTF-1

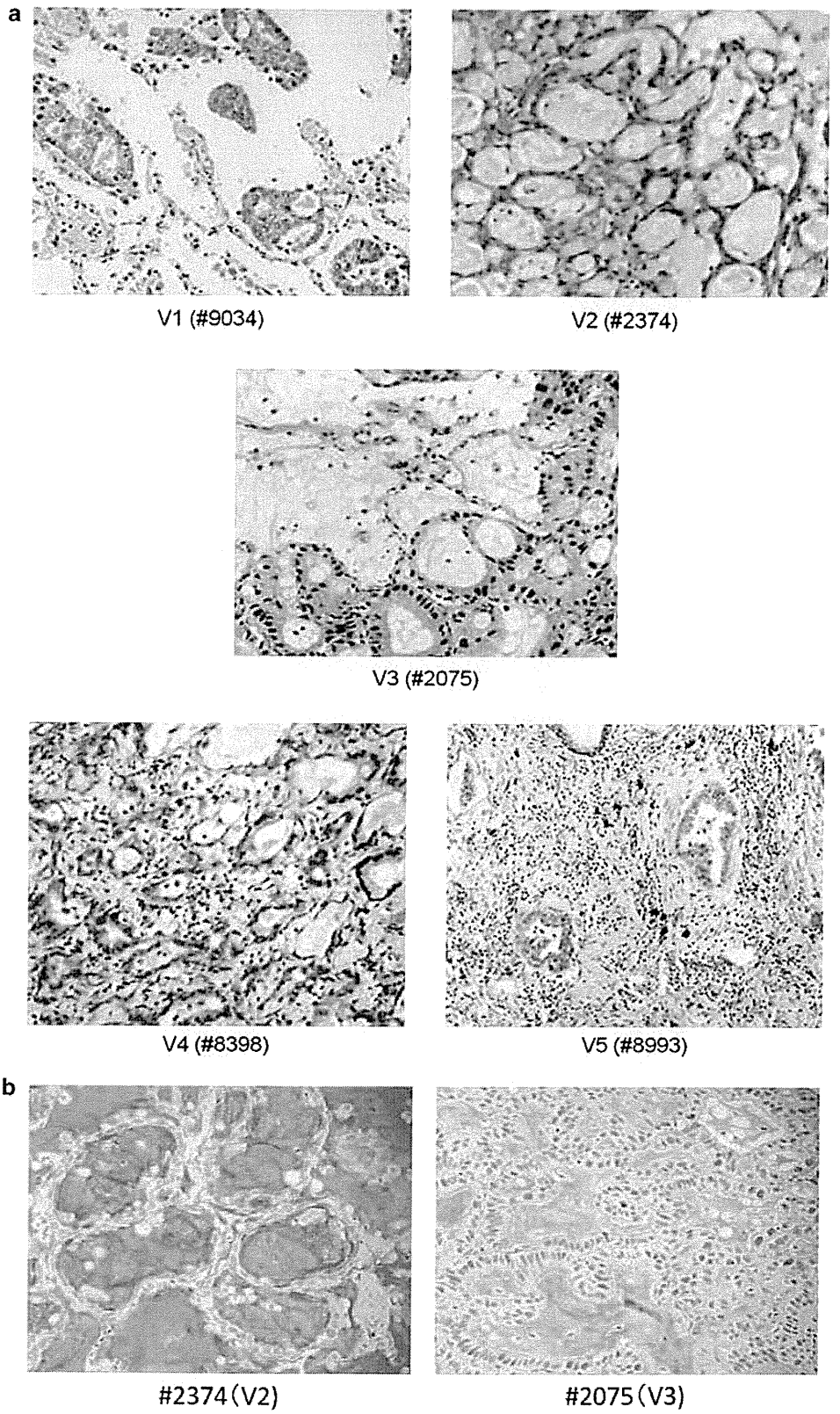

Figure 1 (**a**) Representative appearance of all the five variants of the *EML4-ALK* lung cancers (hematoxylin and eosin staining). Histologically, acinar structures with some mucin production are characteristic. (**b**) Alcian Blue staining shows the abundant mucin production.

Table 3 Clinicopathologic and genetic comparisons between *EML4-ALK* fusion-positive and -negative lung adenocarcinomas

Variables category	*No. of samples (%)*	*EML4-ALK fusion*		P-*value*
		(+) (n = *11)*	*(−)* (n = *242)*	
Age (years; mean ± s.d.)	253	56 ± 11	64 ± 9	0.0062[a]
				0.00038[b]
<50	16 (6.3)	4 (36)	12 (5.0)	
≤50	237 (94)	7 (64)	230 (95)	
Sex				0.61[b]
Males	134 (53)	5 (45)	129 (53)	
Females	119 (47)	6 (55)	113 (47)	
Smoking habit				0.37[b]
Never smokers	105 (41)	6 (55)	99 (41)	
Ever smokers	147 (59)	5 (45)	142 (59)	
Heavy smokers or not				0.040[b]
Heavy smokers	110 (44)	1 (9.1)	109 (45)	
Not heavy smokers	142 (56)	10 (91)	132 (55)	
Tumor size (mm)		20.8 ± 6.7	31.8 ± 16.7	0.031[a]
				0.039[b]
<30	142 (56)	10 (80)	132 (55)	
≥30	111 (44)	1 (20)	110 (45)	
Differentiation grading				0.0082[b]
Well	98 (39)	1 (9.1)	97 (40)	
Less	155 (39)	10 (91)	145 (60)	
EGFR mutation				0.00085[b]
Mutation(+)	41 (52)	0 (0)	41 (60)	
Mutation(−)	39 (48)	11 (100)	28 (40)	
KRAS mutation				0.49[b]
Mutation(+)	7 (10)	0 (0)	7 (12)	
Mutation(−)	61 (90)	11 (100)	50 (88)	
EGFR or *KRAS mutation*				0.00018[b]
Mutation(+)	38 (59)	0 (0)	38 (67)	
Mutation(−)	30 (41)	11 (100)	19 (33)	
p-Stage				0.89[b]
I	143 (57)	6 (55)	137 (57)	
II–IV	110 (43)	5 (45)	105 (43)	

Percentages may not total 100, because of rounding.
We have no smoking history of one patient.
Smoking habits were classified into the following two grades based on the smoking index: (a) non-smokers and light smokers (smoking index <400); and (b) heavy smokers (smoking index = 400 or above).
[a]Student's *t*-test.
[b]Fisher's exact test.

has a decisive role as a master regulatory transcription factor in lung development and in maintenance of the functions of terminal respiratory unit (TRU) cells.[24] The TTF-1 positivity of *EML4-ALK* lung cancers suggests that this subtype might have a TRU histogenesis. TRU-type lung cancers with a TTF-1-positive cell lineage often occur in non- or light smokers, which frequently harbor *EGFR* mutations (61%) and have less-frequent *TP53* mutations (36%) as compared with non-TRU-types (57%).[22] *EML4-ALK* lung cancers also occur in non- or light smokers but do not harbor *EGFR* mutations. The low frequency of *TP53* mutations (9.1%) not only indicates strong oncogenic activity for *EML4-ALK* fusion products but also suggests an independence from smoking, because smoker's adenocarcinomas very frequently harbor *TP53* mutations.[18]

Histologically, less-differentiated acinar structures composed of columnar cells appear characteristic of *EML4-ALK* lung adenocarcinomas. Generally, the columnar cell type is also found in smoker's lung adenocarcinomas, whereas the hobnail cell type, characterized by cytoplasmic protrusions and with a tadpole shape, is often observed in non-smoker's lung adenocarcinomas.[18] Although *EML4-ALK* lung cancers are TTF-1-positive, their histology is

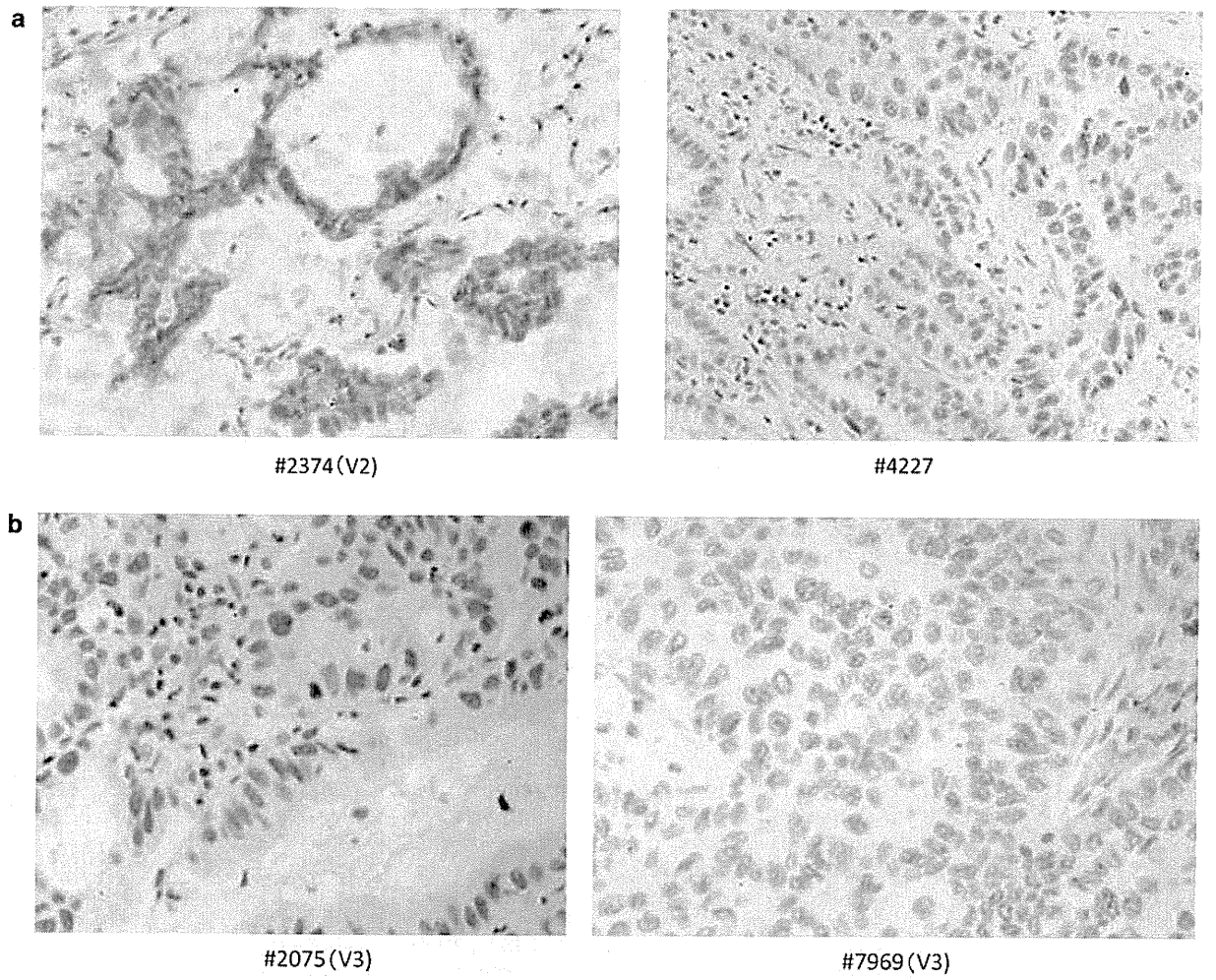

Figure 2 (**a**) Immunohistochemical analysis with a monoclonal anti-ALK antibody of lung adenocarcinoma specimens with (tumor ID #2374) and without (tumor ID #4227) *EML4-ALK* fusion. Note the diffuse staining in the cytoplasm with fine granular accentuation apparent for the *EML4-ALK*-positive tumor. (**b**) Immunohistochemical analysis of lung adenocarcinoma specimens with *EML4-ALK* fusion using a monoclonal anti-TTF-1 antibody. The *EML4-ALK*-positive tumors are partly (ID #2075) or diffusely (ID #7969) positive.

similar to lung cancers developing in smokers, which is interesting in the view of histology–etiology relationships.

Presently, lung adenocarcinomas may be genetically divided into *EGFR*-mutated, *KRAS*-mutated, and *EML4-ALK*-related subtypes. We here elucidated the clinicopathologic, histologic, and genetic characteristics of *EML4-ALK* lung cancers, bearing etiologic implications in mind. Just as some *EGFR*-mutated lung cancers can be successfully treated with EGFR inhibitors, *EML4-ALK* lung cancers may respond to a specific inhibitor treatment, allowing a good prognosis.

Acknowledgement

The authors thank Dr Malcolm Moore for the English correction of the manuscript, and Ms Kazuko Yokokawa, Mr Motoyoshi Iwakoshi, Ms Miyuki Kogure, and Ms Tomoyo Kakita for their technical assistance, and Ms Yuki Takano for her secretarial work. Parts of this study were supported financially by Grants-in-Aid for Scientific Research from the Ministry of Education, Culture, Sports, Science and Technology, from the Japan Society for the Promotion of Science, and by grants from the Ministry of Health, Labour and Welfare, the Smoking Research Foundation, the National Institute of Biomedical Innovation, and the Vehicle Racing Commemorative Foundation, as well as a Grant-in-Aid for Young Scientists (B).

Conflict of interest

K Takeuchi is a consultant providing advisory services to Dako for their antibodies.

References

1 Lynch TJ, Bell DW, Sordella R, *et al.* Activating mutations in the epidermal growth factor receptor underlying responsiveness of non-small-cell lung cancer to gefitinib. N Engl J Med 2004;350:2129–2139.

2 Paez JG, Janne PA, Lee JC, *et al.* EGFR mutations in lung cancer: correlation with clinical response to gefitinib therapy. Science 2004;304:1497–1500.
3 Pao W, Miller V, Zakowski M, *et al.* EGF receptor gene mutations are common in lung cancers from 'never smokers' and are associated with sensitivity of tumors to gefitinib and erlotinib. Proc Natl Acad Sci USA 2004;101:13306–13311.
4 Shigematsu H, Lin L, Takahashi T, *et al.* Clinical and biological features associated with epidermal growth factor receptor gene mutations in lung cancers. J Natl Cancer Inst 2005;97:339–346.
5 Pfeifer GP, Denissenko MF, Olivier M, *et al.* Tobacco smoke carcinogens, DNA damage and p53 mutations in smoking-associated cancers. Oncogene 2002;21:7435–7451.
6 Suzuki H, Takahashi T, Kuroishi T, *et al.* p53 mutations in non-small cell lung cancer in Japan: association between mutations and smoking. Cancer Res 1992;52:734–736.
7 Soda M, Choi YL, Enomoto M, *et al.* Identification of the transforming EML4-ALK fusion gene in non-small-cell lung cancer. Nature 2007;448:561–566.
8 Choi YL, Takeuchi K, Soda M, *et al.* Identification of novel isoforms of the EML4-ALK transforming gene in non-small cell lung cancer. Cancer Res 2008;68:4971–4976.
9 Takeuchi K, Choi YL, Soda M, *et al.* Multiplex reverse transcription-PCR screening for EML4-ALK fusion transcripts. Clin Cancer Res 2008;14:6618–6624.
10 Rikova K, Guo A, Zeng Q, *et al.* Global survey of phosphotyrosine signaling identifies oncogenic kinases in lung cancer. Cell 2007;131:1190–1203.
11 Koivunen JP, Mermel C, Zejnullahu K, *et al.* EML4–ALK fusion gene and efficacy of an ALK kinase inhibitor in lung cancer. Clin Cancer Res 2008;14:4275–4283.
12 Inamura K, Takeuchi K, Togashi Y, *et al.* EML4-ALK fusion is linked to histological characteristics in a subset of lung cancers. J Thorac Oncol 2008;3:13–17.
13 Travis WD, Brambilla E, Muller-Hermelink HK, *et al.* World Health Organization Classification of Tumours: Pathology and Genetics of Tumours of the Lung, Pleural, Thymus and Heart. Springer: Berlin, 2004.
14 Japan Lung Cancer Society. General Rules for Clinical and Pathologic Record of Lung Cancer [in Japanese], 5th edn. Kanahara: Tokyo, 1999.
15 Inamura K, Satoh Y, Okumura S, *et al.* Pulmonary adenocarcinomas with enteric differentiation: histologic and immunohistochemical characteristics compared with metastatic colorectal cancers and usual pulmonary adenocarcinomas. Am J Surg Pathol 2005;29:660–665.
16 Takeuchi K, Choi YL, Togashi Y, *et al.* KIF5B-ALK, a novel fusion oncokinase identified by an immunohistochemistry-based diagnostic system for ALK-positive lung cancer. Clin Cancer Res 2009 (in press).
17 Inamura K, Togashi Y, Nomura K, *et al.* Up-regulation of PTEN at the transcriptional level is an adverse prognostic factor in female lung adenocarcinomas. Lung Cancer 2007;57:201–206.
18 Hashimoto T, Tokuchi Y, Hayashi M, *et al.* Different subtypes of human lung adenocarcinoma caused by different etiological factors. Evidence from p53 mutational spectra. Am J Pathol 2000;157:2133–2141.
19 Stein H, Foss HD, Durkop H, *et al.* CD30(+) anaplastic large cell lymphoma: a review of its histopathologic, genetic, and clinical features. Blood 2000;96:3681–3695.
20 Kosaka T, Yatabe Y, Endoh H, *et al.* Mutations of the epidermal growth factor receptor gene in lung cancer: biological and clinical implications. Cancer Res 2004;64:8919–8923.
21 Noda N, Matsuzoe D, Konno T, *et al.* K-ras gene mutations in non-small cell lung cancer in Japanese. Oncol Rep 2001;8:889–892.
22 Yatabe Y, Kosaka T, Takahashi T, *et al.* EGFR mutation is specific for terminal respiratory unit type adenocarcinoma. Am J Surg Pathol 2005;29:633–639.
23 Shibata T, Hanada S, Kokubu A, *et al.* Gene expression profiling of epidermal growth factor receptor/KRAS pathway activation in lung adenocarcinoma. Cancer Sci 2007;98:985–991.
24 Tanaka H, Yanagisawa K, Shinjo K, *et al.* Lineage-specific dependency of lung adenocarcinomas on the lung development regulator TTF-1. Cancer Res 2007;67:6007–6011.

Int. J. Cancer: **125,** 2836–2843 (2009)

The novel tumor-suppressor Mel-18 in prostate cancer: Its functional polymorphism, expression and clinical significance

Wei Wang[1,2], Takeshi Yuasa[2,3]*, Norihiko Tsuchiya[2], Zhiyong Ma[2], Shinya Maita[2], Shintaro Narita[2], Teruaki Kumazawa[2], Takamitsu Inoue[2], Hiroshi Tsuruta[2], Yohei Horikawa[2], Mitsuru Saito[2], Weilie Hu[1], Osamu Ogawa[4] and Tomonori Habuchi[2]

[1]*Department of Urology, Guangzhou Liuhuaqiao Hospital Guangzhou General Hospital of Guangzhou Military Command, Guangzhou, Guangdong province, China*

[2]*Department of Medical Oncology and Genitourinary Oncology, Cancer Institute Hospital, Japanese Foundation for Cancer Research, 3-10-6 Ariake, Koto-ward, Tokyo, 135-8550, Japan*

[3]*Department of Medical Oncology and Genitourinary Oncology, Cancer Institute Hospital of Japanese Foundation for Cancer Research, 3-10-6 Ariake, Koto-ward, Tokyo, 135-8550, Japan*

[4]*Department of Urology, Kyoto University Graduate School of Medicine, 54 Shogoin Kawahara, Sakyo-ku, Kyoto, 606-8507, Japan*

Mel-18 is a member of the polycomb group (PcG) proteins, which are chromatin regulatory factors and play important roles in development and oncogenesis. This study was designed to investigate the clinical and prognostic significance of Mel-18 in patients with prostate cancer. A total of 539 native Japanese subjects consisting of 393 prostate cancer patients and 146 controls were enrolled in this study. *Mel-18* genotyping was analyzed using a PCR-RFLP method and an automated sequencer using the GENESCAN software. Immunohistochemistry revealed that Mel-18 expression was diminished in high grade and high stage prostate cancers. Moreover, patients with positive Mel-18 expression had significantly longer PSA recurrence-free survival than patients negative for Mel-18 expression ($p = 0.038$). A Mel-18 *1805A/G* SNP was located in the 3' untranslated region and was predicted to alter the secondary structure of the mRNA. *Mel-18* mRNA expression of the 1805*A* allele was clearly higher than expression of the 1805*G* allele by allele specific quantitative RT-PCR. In multivariate analysis, a homozygous *G* allele genotype and negative Mel-18 expression were independent risk factors predicting high PSA recurrence after radical prostatectomy, with HRs of 2.757 ($p = 0.022$) and 2.271 ($p = 0.045$), respectively. Moreover, the *G* allele was also an independent predictor of poor cancer-specific survival with an HR of 4.658 ($p = 0.019$) for patients with stage D2 prostate cancer. This is the first study to provide important evidence demonstrating that Mel-18 is a tumor suppressor and possible therapeutic target, as well as a diagnostic marker for poor prognosis in prostate cancer patients.

Key words: Mel-18; SNP; polycomb group protein; prostate cancer; PCGF2

Polycomb group (PcG) proteins are chromatin regulatory factors that play important roles in development and oncogenesis.[1] Among the PcG family, Bmi-1 is the best characterized protein, and is defined as an oncogene product expressed not only in hematological malignancies but also in various solid tumors.[2–4] Overexpression of Bmi-1-drives an oncogenic pathway demonstrated to lead to a marked propensity for metastatic dissemination as well as a high probability of a poor prognosis in a wide range of cancers including prostate cancer.[5,6] *Mel-18*, which is officially called as PcG RING finger protein 2 (PCGF2), is a member of the PcG gene family whose protein product is structurally highly similar to Bmi-1.[7] Although *Bmi-1* is known to play a role in oncogenesis as a c-*myc* cooperating oncogene, some investigators have reported that *Mel-18* acts as a tumor suppressor *via* transcriptional repression of Bmi-1 and c-Myc.[8–11] *Mel-18* is located at chromosome 17q12, a region associated with prostate cancer risk by previous studies.[12,13]

We hypothesized that Mel-18 may function as tumor suppressor and its expression may alter the clinical behavior of prostate cancer patients. To date, there has been no report investigating the association between Mel-18 and clinicopathological variables of prostate cancer. This study was designed to test our hypothesis and determine the clinical significance of Mel-18 in patients with prostate cancer.

Material and methods

Subjects

A total of 539 native Japanese subjects consisting of 393 prostate cancer patients and 146 controls were enrolled in our study. Control subjects were selected randomly from native Japanese men undergoing a regular medical check-up at the community hospitals in the Akita prefecture. This study was approved by the ethics committee of the Akita University School of Medicine. All of the patients with prostate cancer were treated at these hospitals from April 1997 to December 2003. Written informed consent was obtained from all patients for the use of their DNA and clinical information. The pathological grade and clinical stage of the prostate cancers were determined according to the Tumor-Node-Metastatic system, the Gleason histological grading system and the modified Whitmore-Jewett system, as described previously.[14–17]

Seven renal cancers and surrounding non-cancerous tissues, 8 bladder cancers and surrounding non-cancerous tissues, and 12 non-cancerous prostatic tissues were obtained immediately after resection.

Cell lines were obtained from the American Tissue Type Culture collection (ATCC, Manassas, VA). Two prostate cancer lines, DU145 and PC3, 6 kidney cancer lines, RPMI/SE, CAKI-1, NC65, OSRC2, CCFRC1 and ACHN and 5 bladder cancer lines, 253J, UM-UC-3, TCCSUP, 5637 and KU7, were used for a Mel-18 reverse transcription-polymerase chain reaction (RT-PCR) study.

Immunohistochemical staining

Mel-18 goat polyclonal antibody (Santa Cruz Biotechnology, Inc., Santa Cruz, CA) at a dilution of 1:400 was used as primary antibody. Immunohistochemical staining was performed using a standard avidin-biotin-peroxidase complex method (Histofine, Nichirei, Tokyo, Japan), as described previously.[18]

Additional Supporting Information may be found in the online version of this article.

Grant sponsor: The Takeda Science Foundation, the Kobayashi Institute for Innovative Cancer Chemotherapy, the Shimadzu Science Foundation, the Sagawa Foundation for Promotion of Cancer Research, the Japan-China Sasakawa Medical Fellowship, Grants-in-Aid for Scientific Research from the Ministry of Education, Culture, Sports, Science and Technology, Japan, and the GCOE program of the Ministry of Education, Culture, Sports, Science and Technology, Japan.

***Correspondence to:** Department of Medical Oncology and Genitourinary Oncology, Cancer Institute Hospital of Japanese Foundation for Cancer Research, 3-10-6 Ariake, Koto-ward, Tokyo, 135-8550, Japan. Fax: 81-3-3570-0343. E-mail: takeshi.yuasa@jfcr.or.jp

Received 15 April 2009; Accepted after revision 12 June 2009

DOI 10.1002/ijc.24721

Published online 7 July 2009 in Wiley InterScience (www.interscience.wiley.com).

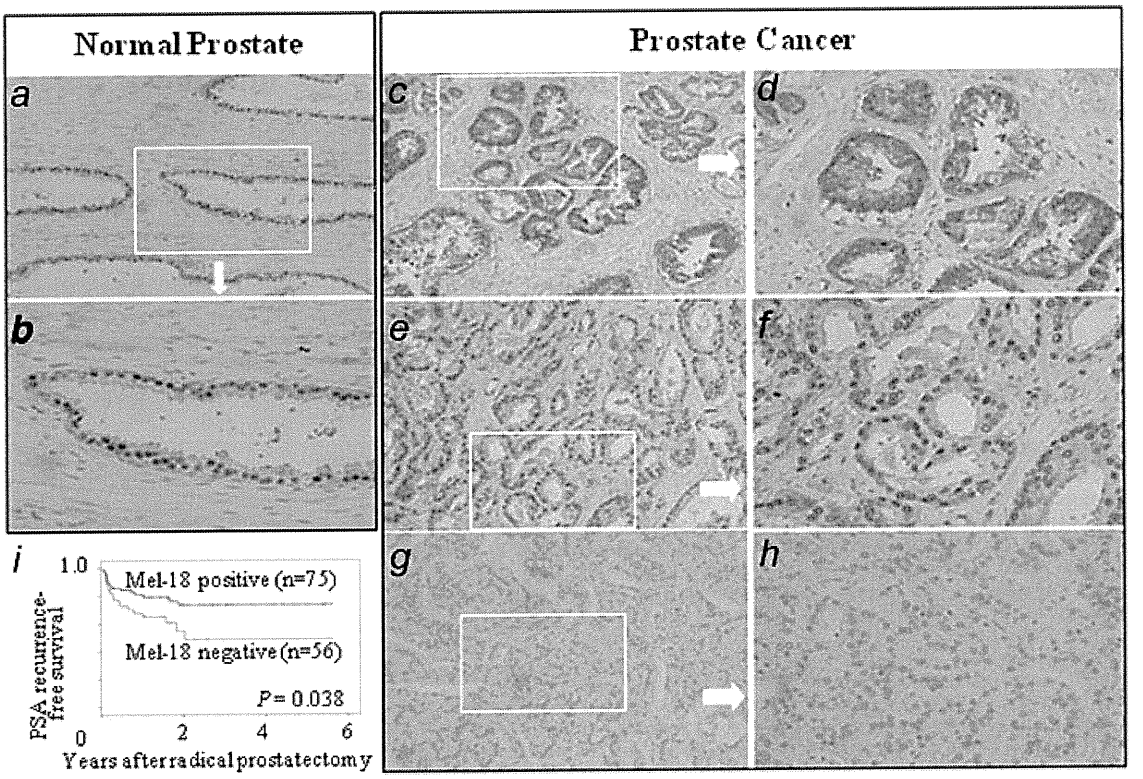

FIGURE 1 – Mel-18 expression and clinical significance. Representative Mel-18 expression in normal (*a,b*) and prostate cancer (*c–h*) tissues. Strong nuclear staining is observed in the non-malignant prostate (*a,b*) whereas various expression patterns including strong (*c,d*), moderate (*e, f*), and weak (*g,h*) expressions, were exhibited by prostate cancer tissues. PSA recurrence-free survival of patients who underwent radical prostatectomy stratified by Mel-18 expression status (*i*).

Immunohistochemical evaluation

Staining results were assessed independently by two investigators (W.W. and M.Z.) in a semi-quantitative fashion at a magnification of 200× (Fig. 1). The staining intensity scores were: 1 (no staining at all), 2 (weak), 3 (medium), and 4 (strong). The staining extent was scored according to the percentage of positive cells: 1 (0% to 5%), 2 (6% to 35%), 3 (36% to 70%), and 4 (71% to 100%). A final score was then calculated by multiplying the above two scores. When the final score was ≥4, the tumor was considered positive for Mel-18 expression; otherwise, the tumor was considered negative. This categorization is fundamentally similar to that used in a previous immunohistochemical study.[10]

Mel-18 genotyping analysis

Mel-18 genotyping was analyzed by a PCR- RFLP method. A 110 bp DNA fragment spanning the *1805A/G* single nucleotide polymorphism (SNP, rs708692) in the *Mel-18* 3′ untranslated region was amplified from genomic DNA. The PCR primer sequences were 5′-TGCTGTCCTGCCTCTGACCAGT-3′ and 5′-CTCAGAACCAGGGATAAACTGCAT-3′. The PCR reactions were performed as described previously.[17] Digestion of the fragment with HpyCH4IV resulted in two fragments of 70 and 40 bp for the *A allele*, and a 110 bp fragment for the *G allele* (Supporting Information Fig. 1). These genotypes were confirmed using GENESCAN software (Applied Biosystems, Foster City, CA).

Measurement of 1805A/G expression of Mel-18

The cDNA from seven cell lines heterozygous for the *1805A/G* polymorphism, including DU145, NC65, CCFRC1, 253J, TCCSUP, 5637 and KU7, was subjected to PCR using primers from the TaqMan® SNP Genotyping Assay kit (ABI Applied Biosystems). The real-time intensity of fluorescence (VIC for 1805*G* and FAM for 1805*A*) was measured using the TaqMan® Gene Expression Master Mix (ABI Applied Biosystems).

Real-time quantitative RT-PCR

The transcriptional levels of *Mel-18*, Bmi-1, c-Myc, and an endogenous control gene (*GAPDH*) were analyzed using the Thermal Cycler Dice™ Real Time System (Takara) with their respective gene specific quantitative real-time RT-PCR primers (Supporting Information Table I), as described previously.[7]

Statistical analysis

Hardy-Weinberg equilibrium analyses were performed to compare the observed genotype frequencies of each category with the expected frequencies using a Chi-square test (degrees of freedom = 1). The age-adjusted odds ratio (aOR) and 95% confidence interval (CI) for the relative risk of prostate cancer and the relationship between the Mel-18 expression or the genotype and histological or clinical variables were determined by multivariate logistic regression analysis with the inclusion of age as a factor. Correlation between gene expression levels was examined using the Spearman coefficient. The survival time was calculated from the date of prostate cancer diagnosis to the date of prostate specific antigen (PSA) recurrence, death from prostate cancer, or death from any cause, for PSA recurrence-free, cancer-specific, and overall survival, respectively. PSA recurrence was defined as the persistence of a post-operative serum PSA level >0.4 ng/ml. PSA recurrence free, cancer-specific, and overall survival were estimated using the Kaplan-Meier method and significant differences in survival were tested using the log rank test. Hazard ratios (HRs) and 95% CIs for cancer death were assessed by the Cox proportional hazard regression model. All of the data were entered into an access database and analyzed using the Excel 2000 or SPSS

TABLE I – CORRELATION BETWEEN MEL-18 EXPRESSION AND CLINICOPATHOLOGICAL FEATURES

Variables	Overall	Mel-18 expression				
		Negative (%)	Positive (%)	*p* Value	Staining score	*p* Value
Overall	131	56 (42.7)	75 (57.3)		5.5 ± 4.2	
Clinical factor						
Age (year)						
−60	14	6 (42.9)	8 (57.1)	0.632	6.2 ± 4.9	0.728
61–70	50	22 (44.0)	28 (56.0)		5.7 ± 4.5	
71–80	61	24 (39.3)	37 (60.7)		5.2 ± 3.8	
81–	6	4 (66.7)	2 (33.3)		4.3 ± 3.6	
PSA (ng/mL)						
0.0–10.0	61	20 (32.8)	41 (67.2)	0.004	6.4 ± 4.4	0.007
10.1–20.0	39	16 (41.0)	23 (59.0)		5.7 ± 4.2	
20.1–100.0	20	10 (50.0)	10 (50.0)		3.9 ± 2.8	
100.1–	11	10 (90.9)	1 (9.1)		2.5 ± 2.3	
Pathological factor						
Pathological stage						
T2N0M0	70	29 (41.4)	41 (58.6)	0.017	6.1 ± 4.6	0.027
T3N0M0	39	12 (30.8)	27 (69.2)		5.5 ± 3.9	
T4< or N1 or M1	22	15 (68.2)	7 (31.8)		3.4 ± 2.3	
Primary Gleason grade						
2,3	65	21 (32.3)	44 (67.7)	0.044	6.3 ± 4.6	0.139
4	53	27 (50.9)	26 (49.1)		4.9 ± 3.7	
5	13	8 (61.5)	5 (38.5)		4.5 ± 3.4	
Gleason score (primary grade + secondary grade)						
5–6	22	4 (18.2)	18 (81.8)	0.023	7.2 ± 5.0	0.026
7	62	27 (43.5)	35 (56.5)		5.8 ± 4.5	
8–10	47	25 (53.2)	22 (46.8)		4.4 ± 3.0	
5–6, 7 (3 + 4)	56	20 (32.8)	41 (67.2)	0.031	6.6 ± 5.0	1.631e-005
7 (4 + 3), 8–10	75	36 (51.4)	34 (48.6)		4.6 ± 3.2	
5–8	99	37 (37.4)	62 (62.6)	0.029	6.0 ± 4.4	0.034
9, 10	32	19 (59.4)	13 (40.6)		4.2 ± 3.1	

(version 10.0J; SPSS, Inc.) software. A probability value of $P < 0.05$ was considered to be statistically significant.

Results

Mel-18 expression and clinical and pathological variables in prostate cancer tissues

First, we examined Mel-18 expression in prostate cancer tissues by immunohistochemistry. In the normal prostatic gland epithelium, strong expression was seen in the nucleus, whereas staining in the cytoplasm was minimal (Figs. 1*a,b*). In contrast, nuclear staining varied among the prostate cancer tissue samples. Typically diminished nuclear expression was frequent in high grade prostate cancer tissues, whereas relatively strong nuclear expression was observed in low grade prostate cancers (Fig. 1*c–h*). In order to clarify the relationship between the clinical and pathological variables and Mel-18 expression, we quantified Mel-18 expression in prostate cancer tissues.

Using immunohistochemistry, we found that histologically low grade and clinically low stage prostate cancers demonstrated significantly higher Mel-18 expression than high grade and high stage cancers (Table I). Significant differences in the Mel-18 staining score relative to serum levels of PSA, pathological stages, and Gleason scores of the patients were detected (Table I). Moreover, patients with positive Mel-18 expression ($n = 75$) had significantly longer PSA recurrence-free survival after radical prostatectomy than patients negative for Mel-18 expression ($n = 56$, $p = 0.038$, Fig. 1*i*).

The mRNA expression of different Mel-18 alleles

We found a *1805A/G* SNP, located in the 3′ untranslated region of *Mel-18* using the NCBI SNP database. The *1805A/G* SNP is predicted to be located at a putative miR-181a binding site by the microRNA binding site prediction software, miRNA Targets (Fig. 2*a*). In addition, according to MFOLD, the mRNA secondary structure prediction tool, the putative secondary structures of the *G* and *A* alleles of *1805A/G Mel-18* differ considerably (Fig. 2*b*).

The *A/G* substitution causes an obvious change in the mRNA, suggesting that this alteration could cause differences in the mRNA stability or protein-translation efficiency (Fig. 2*b*). Therefore, we investigated the expression of each of these *Mel-18* alleles. We used seven urological cancer cell lines, which have a heterozygous *GA* genotype at the *1805A/G* SNP, as described in Material and methods. We found that expression of the *1805A* allele was significantly higher than the *1805G* allele in the seven urological cancer cell lines (Fig. 2*c*) although the expression ratio of *1805A* to *1805G* in the genomic DNA from these heterozygous cell lines was similar (Fig. 2*d*).

Association between the 1805A/G Mel-18 genotype and the risk of prostate cancer

Because the *A* and *G* alleles of *Mel-18* exhibited different levels of expression, we examined the association between the *Mel-18* polymorphism and the risk of prostate cancer. The observed genotype frequency of the polymorphism did not differ from the expected frequency according to the Hardy-Weinberg equilibrium in the control group (data not shown).

The genotype distribution of the *Mel-18 1805A/G* polymorphism is summarized in Table IIA and IIB. There was no significant difference in the genotype distribution between the control and prostate cancer groups (Table IIA). Age-adjusted logistic regression analysis showed no association between the SNP genotype and the risk of prostate cancer (Table IIA). In this genotype analysis, however, we found that the distribution of the *AA* genotype was significantly higher in histologically low or intermediate grade and clinically localized prostate cancers than in the high grade and metastatic cancers (Table IIB).

The association between the Mel-18 polymorphism and cancer progression after radical prostatectomy

Next, we examined the association between the *Mel-18* polymorphism and cancer progression after radical prostatectomy. The

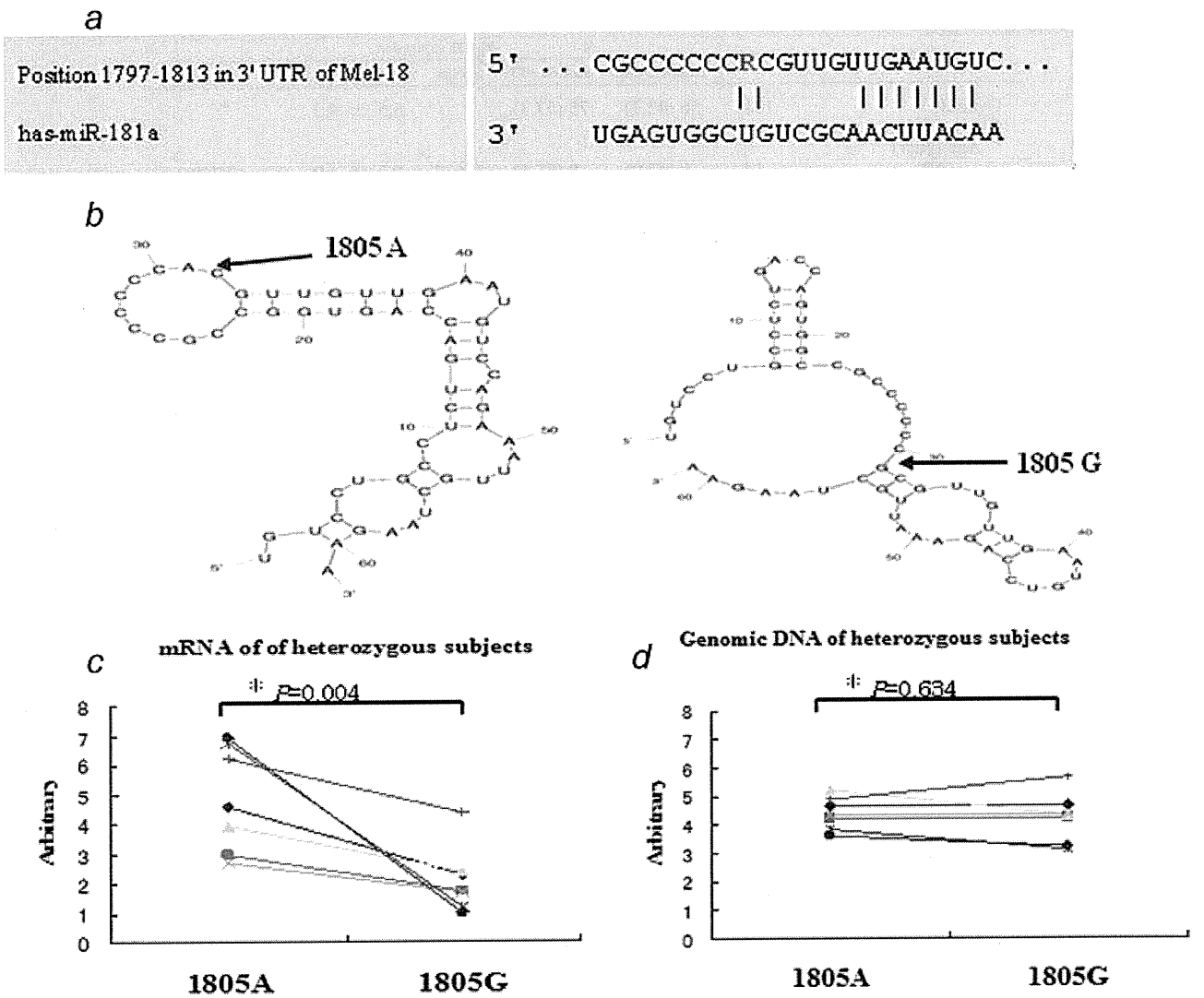

FIGURE 2 – *Mel-18 1805A/G* polymorphism and clinical significance. (*a*) The *Mel-18* 3′ UTR contains a miR-181a binding site. Schematic microRNA binding site structures for the *1805A/G* alleles. (*b*) *Mel-18* mRNA folding structures predicted by MFOLD. (*c*) The mRNA expression for the *1805A* and *1805G* alleles in the *1805A/G* heterozygous cell lines including DU145, NC65, CCFRC1, 253J, TCCSUP, 5637, and KU7. (*d*) Quantitation of the control products amplified from genomic DNA (*$p = 0.004$). [Color figure can be viewed in the online issue, which is available at www.interscience.wiley.com.]

mean age ± SD of the 124 patients who underwent radical prostatectomy was 70.2 ± 5.1 years. The mean follow-up period was 36.3 ± 22.8 months. The mean preoperative serum PSA was 17.0 ± 14.9 ng/ml.

The distribution of clinical stages of these patients, T1, T2, and T3 was 45 (36.3%), 58 (46.8%) and 21 (16.9%), respectively. The distribution of pathological stages, pT2, pT3, and pT4 was 73 (58.9%), 43 (34.7%), and 8 (6.5%), respectively, and a positive surgical margin was observed in 76 (61.3%) cases. A Gleason sum score of <7, 7, and >7 was present in 25 (20.2%), 52 (41.9%) and 47 (37.9%), respectively. The 3- and 5-year PSA recurrence-free survival rates were 66.8% and 37.9%, respectively, with a median survival time of 58.1 months. Kaplan-Meier survival curves stratified by *Mel-18* genotype demonstrated that patients with the *GG* genotype had a significantly higher rate of PSA recurrence compared to the *AA* or *GA* genotype ($p = 0.002$, Fig. 3*a*).

Univariate analysis of the PSA recurrence-free survival stratified by dichotomized groups for each factor showed that PSA = 9.6 ($p = 0.003$), pathological T status =T3 ($p < 0.001$), positive surgical margin ($p < 0.001$), the *GG* genotype ($p = 0.004$), and negative Mel-18 expression ($p = 0.042$) were each significantly associated with poor survival (Table IIIA). In a multivariate analysis, higher PSA level, positive surgical margin, the presence of the *GG* genotype, and negative Mel-18 expression were independent risk factors predicting PSA recurrence after radical prostatectomy, with HRs of 3.095 (95% CI, 1.352–7.083; $p = 0.007$), 4.759 (95% CI, 1.857–12.191; $p = 0.001$), 2.757 (95% CI, 1.154–6.588; $p = 0.022$) and 2.271 (95% CI, 1.018–5.066; $p = 0.045$), respectively (Table IIIA).

Association between the Mel-18 polymorphism and survival in patients with metastatic prostate cancer

Next, we examined the association between the *Mel-18* polymorphism and survival of metastatic prostate cancer patients. The mean age ± SD of the 66 patients with bone metastases at diagnosis was 72.6 ± 8.5 years. The mean follow-up period was 53.3 ± 38.9 months. The 5-year overall survival rates were 52.2 months, with a median survival time of 64.8 months.

Survival was compared between the two groups divided according to the *Mel-18* genotype, *i.e.*, patients with the *AA*

TABLE II – GENOTYPE FREQUENCIES OF THE MEL-18 SNPS AND AGE-ADJUSTED ODDS RATIO

Mel-18 1805A/G Genotype	Male controls *n* (%)	Prostate cancer *n* (%)	aOR[1] (95% CI[2])	*p*
(A) Comparison of prostate cancer patients with male controls				
Mel-18 1805 A/G	146	393		
AA	71 (48.6%)	170 (43.3%)	ref	
GA	60 (41.1%)	179 (45.5%)	1.254 (0.837–1.879)	0.273
GG	15 (10.3%)	44 (11.2%)	1.238 (0.642–2.362)	0.532
GA + *GG* (against *AA*)	75 (51.4%)	223 (56.7%)	1.248 (0.851–1.830)	0.256
GA + *AA* (against *GG*)	131 (89.7%)	349 (88.8%)	0.907 (0.487–1.690)	0.758
Mel-18 1805A/G Genotype	Stage[3]		aOR[1] (95% CI[2])	*p*
	Localized	Metastatic		
(B) Comparison of patients with high stage or high grade prostate cancers to patients with low stage or low grade prostate cancers				
AA	139 (47.4%)	31 (31.0%)	ref	
GA	126 (43.0%)	53 (53.0%)	1.792 (1.071–2.999)	0.026
GG	28 (9.6%)	16 (16.0%)	2.409 (1.148–5.058)	0.020
GA + *GG* (against *AA*)	154 (52.6%)	69 (69.0%)	1.906 (1.166–3.115)	0.010
GA + *AA* (against *GG*)	265 (90.4%)	84 (84.0%)	0.573 (0.292–1.126)	0.106
Mel-18 1805A/G Genotype	Grade[4]		aOR[1] (95% CI[2])	*p*
	Low + Intermediate	High		
AA	108 (47.0%)	57 (36.3%)	ref	
GA	101 (43.9%)	77 (49.0%)	1.517 (0.971–2.371)	0.067
GG	21 (9.1%)	23 (14.6%)	2.272 (1.146–4.508)	0.019
GA + *GG* (against *AA*)	122 (53.0%)	100 (63.7%)	1.646 (1.076–2.517)	0.022
GA + *AA* (against *GG*)	209 (90.9%)	134 (85.4%)	0.549 (0.289–1.041)	0.066

[1]Age-adjusted odds.–[2]95% confidence interval. –[3]Localized, stage A–C; metastatic, stage D.–[4]Low, well-differentiated or Gleason score 2–4; intermediate, moderately differentiated or Gleason score 5–7; High, poorly differentiated or Gleason score 8–10.

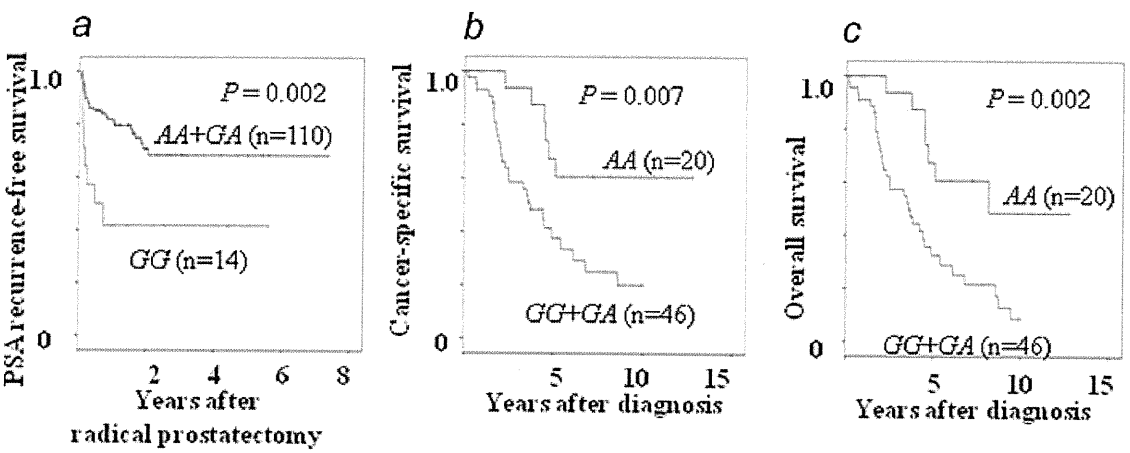

FIGURE 3 – Association between the *Mel-18* polymorphism and survival in patients with prostate cancer. Kaplan-Meier curves of PSA recurrence-free survival in patients with prostate cancer who underwent radical prostatectomy (*a*). Kaplan-Meier curves of cancer-specific survival (*b*) and overall survival (*c*) in patients with prostate cancer and bone metastasis at initial diagnosis. [Color figure can be viewed in the online issue, which is available at www.interscience.wiley.com.]

genotype (n = 20) and with the *GA* or *GG* genotype (n = 46). The *AA* genotype was associated with significantly better cancer-specific and overall survival compared with the *GA* or *GG* genotype (p = 0.007 and p = 0.002, respectively; Fig. 3*b* and 3*c*). The 5-year overall survival rates were 48.3% for patients with the *GA* or *GG* genotype and 69.2% for patients with the *AA* genotype. The median cancer-specific survival time of patients with the *GA* or *GG* genotype was 46.9 months and with the *AA* genotype 81.6 months. The median overall survival time of patients with the *GA* or *GG* genotype was 48.9 months and with the *AA* genotype was 76.9 months.

In a univariate analysis, age (p = 0.044), pretreatment PSA level (p = 0.002), levels of hemoglobin (p < 0.001), alkaline phosphatase (p < 0.001), and lactate dehydrogenase (p = 0.030), as well as *Mel-18* polymorphism (p = 0.011), were significantly associated with cancer-specific survival. A multivariate analysis revealed that the Mel-18 *A* allele (p = 0.019), elevated serum PSA (p = 0.037), and elevated serum alkaline phosphatase (p < 0.001) were independent predictors of poor cancer-specific survival (Table IIIB).

Mel-18 expression and the Mel-18 1805A/G genotypes

We examined the association between Mel-18 expression and *Mel-18 1805A/G* genotype in patients with prostate cancer. The patients with the *Mel-18* 1805 *AA* genotype tended to have higher